

Chapter 1

Literature Review

1.1 Extrasolar Planets	3
1.1.1 Overview	3
1.1.2 Observation Techniques	4
Radial velocities	4
Transits	5
Direct imaging	5
Gravitational microlensing	6
Timing	6
Astrometry	6
1.1.3 State of the Field – Challenges and Future Perspectives	7
The search of low-mass planets	7
Precise characterization of exoplanets	7
1.2 Stellar Activity and Noise	9
1.2.1 Magnetic Fields at a Glance	9
Babcock–Leighton magnetic dynamo model	10
Modern perspective of magnetic dynamo model	11
1.2.2 Sunspots and Starspots	12
Sunspots	12
Starspots	12
1.2.3 Faculae	12
1.2.4 Plages	13

1.2.5	Granulation	15
1.2.6	Flares	15
1.2.7	Stellar Oscillations	17
1.2.8	Solar Surface Magneto-Convection	17
	Condition of convection	17
	Topology of convection	18
	Hierarchical structure of convection	18
	Magnetic fields come into play	19
1.3	The Challenge of Finding Exoplanets in the Presence of Stellar Noise	20
1.3.1	The Amplitudes and Time-scales of Stellar Jitter	20
	Minutes: stellar oscillations	20
	Minutes to hours: granulation	21
	Minutes to hours: flares	22
	Days: starspots, faculae, plages	22
	Decades: magnetic cycles	23
	Varying time-scale: gravitational redshift	24
	Varying time-scale: binary companions	25
1.3.2	The Properties of Stars as a Function of Spectral Type	25
	Hot stars	26
	Red giants	26
	F5 to M5 stars	26
	Cool stars	26
1.3.3	Two Components of Radial Velocity Shifts	27
1.3.4	Observational Methods for Detection and Quantification of Stellar Activity	27
	Cross correlation function	27
	Measure of spectral line profile deformation	28
	Activity indicators from spectral lines	29
	Photometry	31
	Lomb-Scargle periodogram	32
1.3.5	Summary	33
1.4	References	34

1.1 Extrasolar Planets

1.1.1 Overview

Exoplanet research is undoubtedly the youngest and the most rapidly developing field in astrophysics. The first confirmed exoplanetary system was discovered by the Polish astronomer Aleksander Wolszczan and the Canadian astronomer Dale Frail back in 1992, based on precise timing measurement of the millisecond pulsar PSR B1257+12 [139]. The first discovery of exoplanet orbiting around a main-sequence star was made in 1995, by the Swiss astronomers Michel Mayor and Didier Queloz, using the precise radial velocity measurement of the metal-rich G2V type host star 51 Pegasi [86].

Since then, the field of exoplanet discovery has been flourishing, especially in recent years. To date ¹, 3576 exoplanets, including 2686 planetary systems and 602 multiple planet systems have been confirmed, most of which were found using the radial velocity method and the transits method (Fig. 1.1, § 1.1.2).

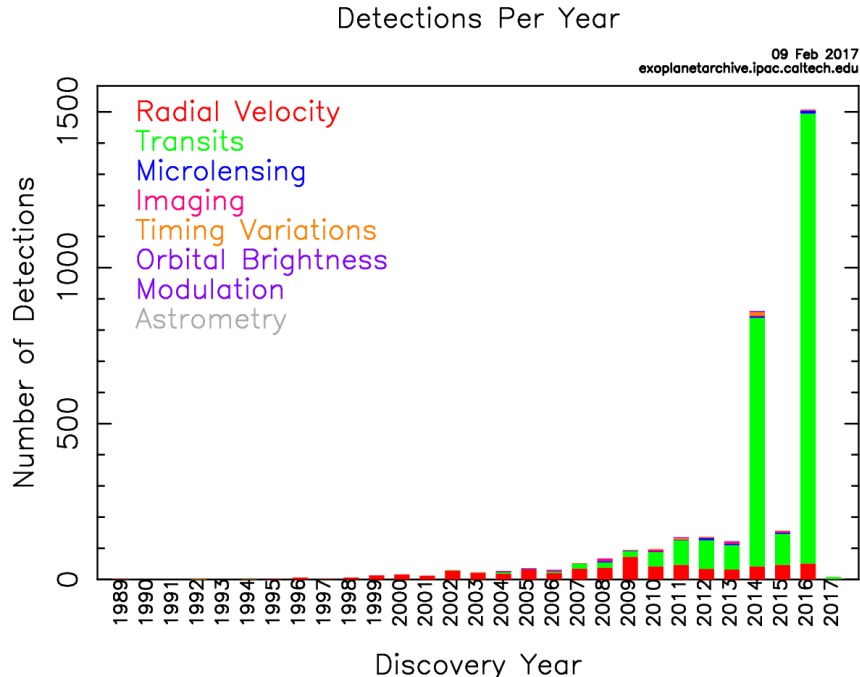


Fig. 1.1: Rapidly developing history of exoplanet discovery, classified by detecting methods. [9]

¹ 14 Feb, 2017

1.1.2 Observation Techniques

Radial velocities Radial velocity was the most widely used technique before the Kepler era and it remains one of the most successful planet detection techniques. In a planetary system, the star follows a reflex motion around the system barycentre, and its velocity periodically oscillates along the line-of-sight with respect to an observer. The velocity oscillation of the host star results in the Doppler shift of the stellar spectrum, which can be recorded by a high-resolution spectrograph. To obtain precise radial velocities, high spectral resolution ($R = \lambda/\Delta\lambda \sim 50\,000 - 100\,000$), high instrumental stability and accurate wavelength calibration are required [102].

For a planet of mass M_p , orbiting the host star of mass M_\star , with the orbital period P and inclination of the orbital plane i , the stellar radial velocity semi-amplitude can be expressed as

$$K = 28.4 \text{ ms}^{-1} \left(\frac{P}{1 \text{ yr}} \right)^{-\frac{1}{3}} \left(\frac{M_p \sin i}{M_J} \right) \left(\frac{M_\star}{M_\odot} \right)^{-\frac{2}{3}}, \quad (1.1)$$

which gives $K_J = 12.5 \text{ m s}^{-1}$ for Jupiter and $K_\oplus = 0.09 \text{ m s}^{-1}$ for Earth around the Sun [102].

Radial velocities are more sensitive to close-in (short orbital period P), massive (large M_p) planets around low-mass stars (small M_\star) in edge-on (large $\sin i$) planetary systems, and thus deliver a large population of gas-giants (e.g. 51 Pegasi² [86], v Andromedae³ [28]) and Neptune-sized (e.g. HD 69830⁴ [80]) planets. At $\sim 1 \text{ m s}^{-1}$ precision, the *High Accuracy Radial Velocity Planet Searcher* (HARPS), has also been able to detect super-Earths (e.g. HD 85512⁵ [101], Wolf 1061⁶ [140]) and even earth-sized planets (e.g. Proxima Centauri b⁷ [5]). It is also capable of detecting multi-planet systems in the pursuit of sub-meter precision detection, such as HD 10180 – the most prolific exoplanet system, with up to seven planets discovered to date [81].

²A hot Jupiter – the first exoplanet around a solar-type star.

³Three gas giants – the first identified multi-planet system.

⁴Three Neptunes within 0.6 AU – the first system of low-mass planets.

⁵0.7 m s⁻¹ radial velocity amplitude.

⁶Wolf 1061c is the second-closest known potentially habitable exoplanet.

⁷Its host, the red dwarf star Proxima Centauri, is the closest star to the Sun.

Given the scope of this thesis, we will focus on a discussion of radial velocities, and only briefly introduce other detecting methods below.

Transits When an exoplanet passes in front of its host star (i.e. transits), it blocks a fraction of the stellar flux. This can be detected as a dip in the transit light curve. A secondary eclipse, or occultation, can also occur when the planet passes behind the star, resulting a smaller drop in the combined flux of the system. Transits provide information on the radii of the transiting planet. Combined with radial velocity observations which provide information on mass, the two techniques together deliver the density of the planet. This is crucial in determining the architecture of the exoplanet. Photometric and spectroscopic observations of transits and eclipses can further probe the atmospheric properties of the planet.

In a multiplanetary system, the transiting planet not only response to the gravitational influence of the host star, but is also dynamically perturbed by other planets in the system. This can cause a transiting planet to transit earlier or later than if it were a single planet system. The measurement of transit timing variations (TTV) provides data on the mass as well as size of the planet (e.g. TRAPPIST-1 [52]).

Direct imaging refers to the direct detection of exoplanets, either through reflected light from the host star, or the planet's infrared thermal emission. It is extremely difficult even for today's 10 meter class telescopes to detect planets of interest. Major challenges include but are not limit to: (1) small planet-star flux ratio ($\sim 10^{-5} - 10^{-10}$ from infrared to optical); (2) small star-planet angular separation (within 0.1-0.5 arcsec); and (3) atmosphere phase fluctuation. A combination of the following techniques have been employed to deal with these challenges: (1) coronagraphically mask to suppress the glare of the star at the telescope focal plane; (2) eliminate stellar light with nulling interferometry; (3) use large-aperture or long-baseline telescopes to increase spacial resolution; (4) adaptive optics: measure the wavefront of a bright reference star to perform wavefront correction to achieve diffraction limited resolution.

Gravitational microlensing Gravitational microlensing can be detected when a background light source (usually a star in the Galactic bulge region), a foreground lens (e.g. a planetary system) and an observer are aligned within the angular Einstein radius (\sim milliarcseconds). Light beams from the source are bent and enhanced by the host star and the planets individually. Such a microlensing light curve can deliver estimates of mass and orbital radius of the components of a planetary system. However, due to its nature of occurrence, the probability of such events are very small and the observation is non-repeatable.

Timing Systems such as pulsars, eclipsing binaries and pulsating stars show periodic signals. In the presence of exoplanets, the timing interval will be modulated due to variation in the light travel time to the observer. For example, the first exoplanet PSR B1257+12 B was discovered using this method [139]. Thanks to the short (\sim milliseconds) and stable periods of pulsars, this method was sensitive enough to detect the lowest-mass planet found to date, PSR B1257+12 A, with 0.02 Earth mass or twice the mass of the Moon [70]. A second unique example concerns the recent discovery of the first main-sequence A-star known to host a Jupiter-mass planet around the habitable zone [90]. It suggested a new way of looking for exoplanets around hot and pulsating stars, which is not obtainable from radial velocity detections due to lack of spectral lines.

Astrometry Astrometry is the measurement of positions and motions of celestial bodies projected onto the sky. In the field of exoplanet searches, it can detect the motion (i.e. wobbles in the transverse direction) of a star perturbed by orbiting planets.

ESA launched the space mission *Global Astrometric Interferometer for Astrophysics* (Gaia) in 2013 [51]. It is dedicated to astrometric measurements with high accuracies ($\sim 20 - 25$ microarcsecond at $V = 15$ mag) and expected to deliver some 21,000 planets within 500 pc in the solar vicinity using astrometry [103]. It is a complementary technique to radial velocity and transit observations, and is most sensitive to face-on systems and widely separated planets.

1.1.3 State of the Field – Challenges and Future Perspectives

With the discovery of dramatically increasing number of exoplanets (Fig. 1.1), the focus of interest has gradually shifted to the following two areas: (a) the search for low-mass planets, and (b) precise characterization of exoplanets [85]. Both are driven by the underlying pursuit of earth-sized planets in the habitable zone.

The search of low-mass planets Radial velocity observations measure the overall shift of spectral lines recorded in a spectrograph. Precisions of m s^{-1} and even sub- m s^{-1} are reachable using the state-of-the-art spectrographs today. These offer the possibility of detecting smaller and smaller radial velocities induced by orbiting planets. However, such radial velocity shifts are also sensitive to intrinsic stellar variability which acts as a source of radial velocity noise (§ 1.2). Such variability can have similar amplitudes, and can thus strongly obscure, the detection of low-mass exoplanets [40]. The system GJ667C, for example, has shown an inconsistency in the number of exoplanets claimed by various teams of researchers ([46], [6], [58]). There has been ongoing debates regarding Alpha Centauri Bb, an exoplanet claimed to be detected in the closest star system to our Solar System, on whether the radial velocity oscillation was a result of an orbiting planet, or simply spurious signals from the star that mimic the presence of a planet ([41], [110], [61]). Therefore, it is fundamental for today’s extreme precision exoplanet searches, to extract low-amplitude planet signals in the presence of stellar noise. This is the primary motivation of this thesis (§ 1.3).

Precise characterization of exoplanets Radial velocity observations are crucial to (a) confirming the exoplanet candidate from transit surveys and (b) understanding the planet properties. The *Kepler* mission has been extraordinarily successful in delivering a larger number of exoplanet candidates than any other surveys. However, the faintness of Kepler targets largely limits their radial velocity follow-up. Without additional information from radial velocity measurements, e.g. the planet mass, the complete characterization of the exoplanet is not possible. Future space missions such as NASA’s *Transiting Exoplanet Survey Satellite* (TESS) [114] and ESA’s *PLAnetary Transits and*

Oscillations of stars (PLATO) [111] will effectively solve this problem, by delivering bright stars for radial velocity follow-up. For low-mass planets around nearby stars, radial velocities will be more advantageous in the sense that it can be sensitive to the Doppler wobbling of the star even if the planets never transit due to the orbital plane configuration. In such cases, we rely on direct-imaging to characterize the atmospheric properties of these planets [40].

1.2 Stellar Activity and Noise

Stars spend most of their lifetime in hydrostatic equilibrium, meaning the inward pull of gravity is balanced with the outward force due to gas pressure gradient. For main-sequence stars, hydrogen is burnt into helium through nuclear fusion, releasing the energy in a relatively steady state. Radiation and convection play a vital role in the transportation of energy. For the Sun, energy generated at the central core region (25% of solar diameter) is transported via radiation in the radiative zone (extending from the core to 75% of solar diameter) and then brought up to the surface by convection, where it radiates away (Fig. 1.2). The dynamics of the stellar surface, combined with the effect of magnetic fields, are the underlying cause of stellar inhomogeneities, such as granules, starspots and faculae in the photosphere; plages and prominences in the chromosphere.

In this section, we will investigate the physics of a selection of stellar inhomogeneities and their impact on radial velocity detection of exoplanets.

1.2.1 Magnetic Fields at a Glance

Generally speaking, magnetic fields are produced by moving charged particles. For stars, the “fuel” for magnetic fields is plasma – gas that is heated to such high temperature

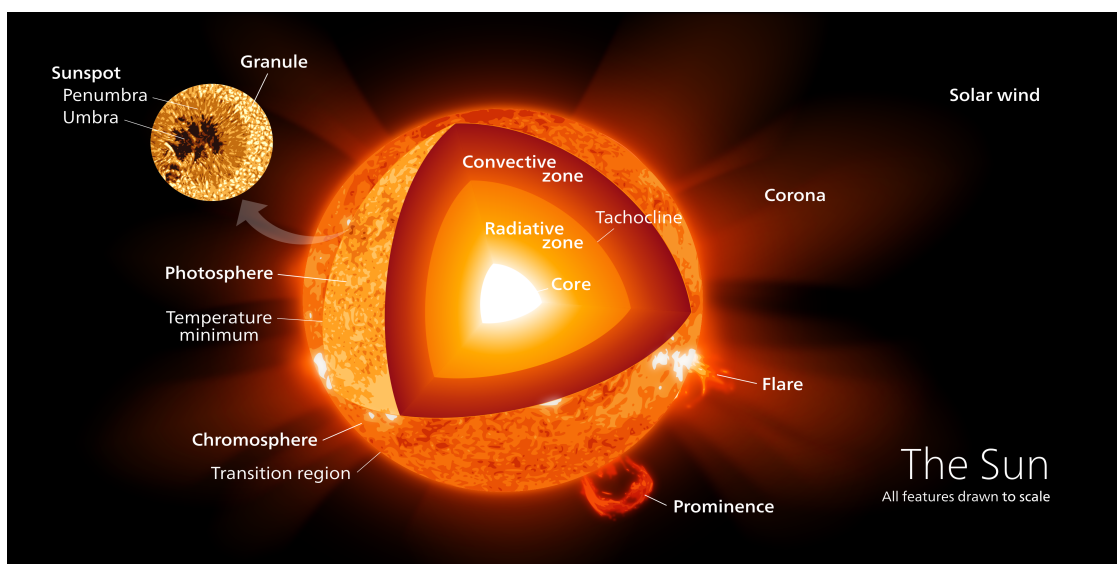


Fig. 1.2: Schematic interior structure of the sun. Courtesy of Wiki user: Kelvin13.

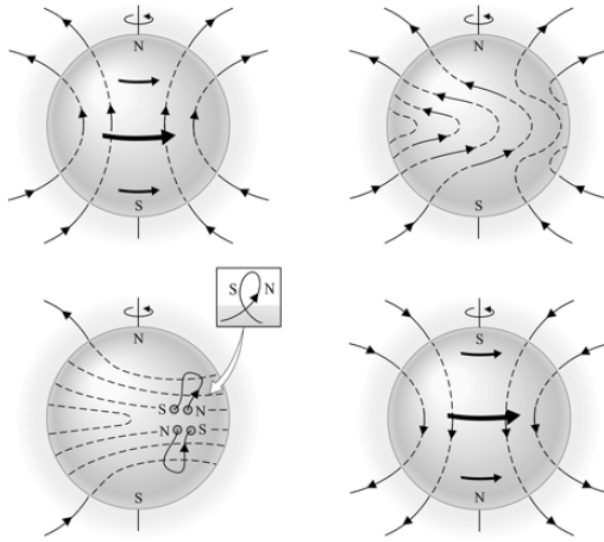


Fig. 1.3: A schematic view of the solar magnetic dynamo model.

that the atoms are ionized into ions and electrons. The plasma motion can be driven by the density and temperature gradient of the star, and it is further complicated by the stellar rotation. Cool stars with convection envelopes like our Sun are known to produce substantial magnetic fields, leading to stellar activities [18].

Babcock–Leighton magnetic dynamo model Babcock proposed a magnetic dynamo model that described the origin of solar magnetic field [13], which was later elaborated by Leighton ([75], [76]). As depicted in Fig. 1.3, the magnetic fields are initially poloidal, and the magnetic field lines are “frozen” into the plasma in an ideally high conductivity case. The differential rotation of the Sun drags the plasma along with the magnetic field lines and produces a significant toroidal component to the poloidal field. The magnetic field lines are then disrupted by the turbulent convective zone. They are twisted to become magnetic ropes, generating intense magnetic fields. The magnetic pressure $P_m = B^2/(2\mu_0)$ changes as a result, generating buoyancy that causes the ropes to rise to the surface to produce sunspots (§ 1.2.2).

It is observed that the Sun undergoes an 11-year solar cycle, i.e. the cyclic sunspot minimum and maximum shown in the butterfly diagram (Fig. 1.4). The Babcock–Leighton model also provided an explanation of the solar cycle. At the beginning

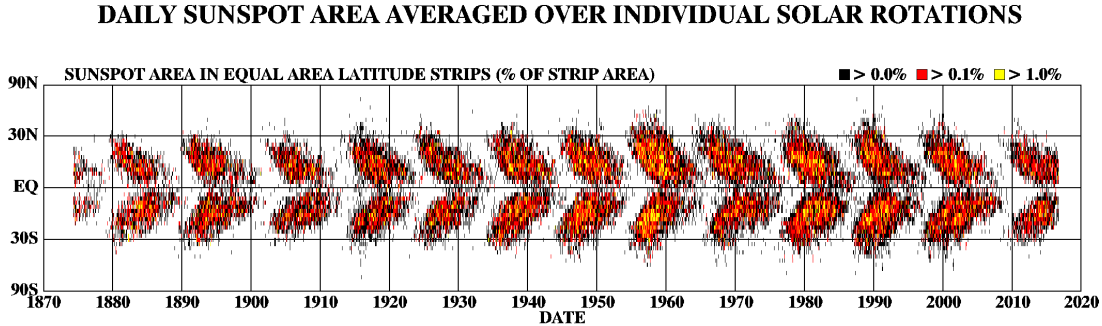


Fig. 1.4: Sunspot butterfly diagram shows the evolution of sunspots in a 11-year cycle. Courtesy of Solar group at NASA Marshall Space Flight Centre.

of the cycle, twisting of magnetic field lines occurs in higher latitudes, which corresponds to the sunspot minimum. More sunspots develop in intermediate latitudes as a result of differential rotation further dragging the field lines into knots. This corresponds the sunspot maximum. In the end, sunspots from two hemispheres cancel each other out, when the sunspots in pairs with opposite polarities come to merge near the equator. Such cancellation of magnetic fields is followed by the re-establishment of a poloidal field, causing the polarity reversed (Fig. 1.3). Hence, the complete magnetic cycle is 22 years, when the flip of polarities are taken into account.

Modern perspective of magnetic dynamo model The solar dynamo model explains the origin of solar magnetic fields and the magnetic cycle, however, it has yet to answer more detailed questions regarding stellar activity, and it is questionable whether our knowledge and investigation of the solar magnetic activity will lead to the corresponding understanding of stellar dynamos and stellar activity in general [113]. A more complete picture of the solar dynamo model can be obtained with the treatment of magnetohydrodynamical (MHD) induction equations and MHD simulations, as discussed in [32] and [45].

It is now widely accepted that magnetic fields are generated by the magnetic dynamo in the tachocline, an interface layer between the radiative zone and the convective zone, where rotation rate changes rapidly. The tachocline plays an important role in the magnetic dynamo ([97], [53]): (a) it stores the induced toroidal field, whereas the convective zone above has little capacity and the radiative zone below traps the field;

(b) the toroidal field B_{tor} is responsible for generating a new poloidal field B_{pol} by the α effect: $\delta B_{\text{pol}}/\delta t = \alpha B_{\text{tor}}$; (c) it enhances the induction of both poloidal and toroidal fields thanks to the low turbulent diffusivity in the tachocline.

1.2.2 Sunspots and Starspots

Sunspots As discussed in § 1.2.1, sunspots are direct consequences of local magnetic fields. Magnetic fields suppress the convective motion at the surface, blocking the outflow of energy, resulting in cooler and darker regions. For this reason, sunspots appear as dark spots on the solar surface, with temperatures ~ 3500 K compared with ~ 5500 K in the surrounding photosphere. The magnetic field is stronger and vertical in the central darker portion (i.e. umbra) and it is weaker and inclined in the lighter surroundings noticeable as a filament-like structure (i.e. penumbra) (Fig. 1.2).

Starspots Starspots are the equivalent of sunspots, observed in other stars. Sunspots and starspots provide an important clue of internal dynamo activity and complex magnetic field structure. Zeeman splitting of spectral lines can also be observed in the presence of strong magnetic fields in starspots. Using the Zeeman Doppler Imaging (ZDI) technique, the magnetic topography of the stellar surface can be reconstructed (e.g. [39], [48]). Recently for the first time, observations with the long-baseline infrared interferometry on ζ Andromedae, a nearby active old star, showed that the star harboured spots in the northern polar region and across lower latitudes [120]. Such unique spot configurations pose again the challenge of applying our knowledge of spot formation beyond the Sun.

1.2.3 Faculae

Faculae are slightly brighter regions in the photosphere associated with strong magnetic fields on a smaller scale. They are the second most obvious feature on the solar disk, after sunspots (Fig. 1.5). Interestingly at sunspot maximum, the large number of extended

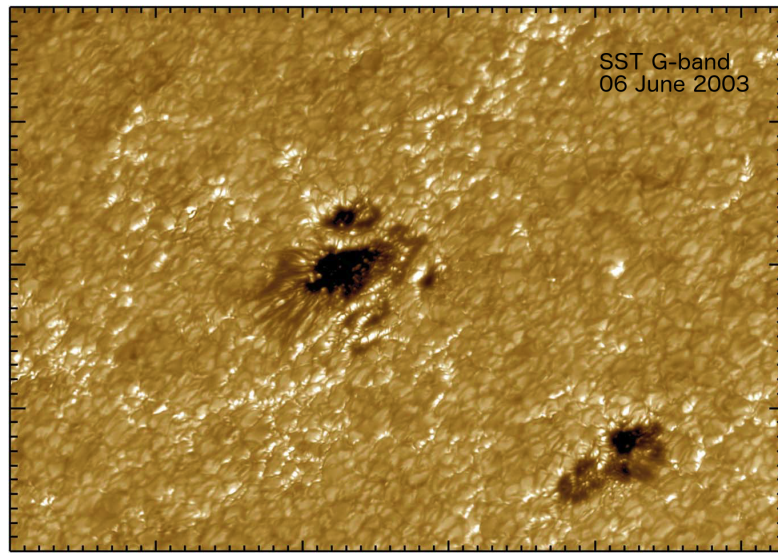


Fig. 1.5: High resolution images of faculae, seen as the bright structures in the extended region near the sunspots. Scale: 1 000 km per hatch mark. Courtesy of Swedish one-meter Solar Telescope.

faculae makes up for the flux deficit of sunspots, so that the total irradiance of the Sun appears slightly higher than at sunspot minimum ([50], [71], [136]).

An explanation of the origin of faculae was first proposed by Spurit in 1976, known as the *Bright Wall* model. He explained that gas pressure became lower as exerted by magnetic field, thus causing the gas to be less opaque than the surroundings, allowing the observer to see deeper into the photosphere ([125], [126]). The modern explanation is in favour of the *Bright Wall* model, in a sense that the reduced opacity in the magnetic flux provides an insight to the non-magnetic granule. Numerical magnetohydrodynamics simulations based on this prototype has been successful in reproducing the observed faculae structures [68].

1.2.4 Plages

Plages are the counterpart of faculae in the chromosphere. They are also a product of strong local magnetic fields, characterized by the bright H α emissions found near the sunspots. They can be used as tracer of imminent solar activities, as they emerge before and disappear after the sunspots [29]. The expansion of plages also tend to map

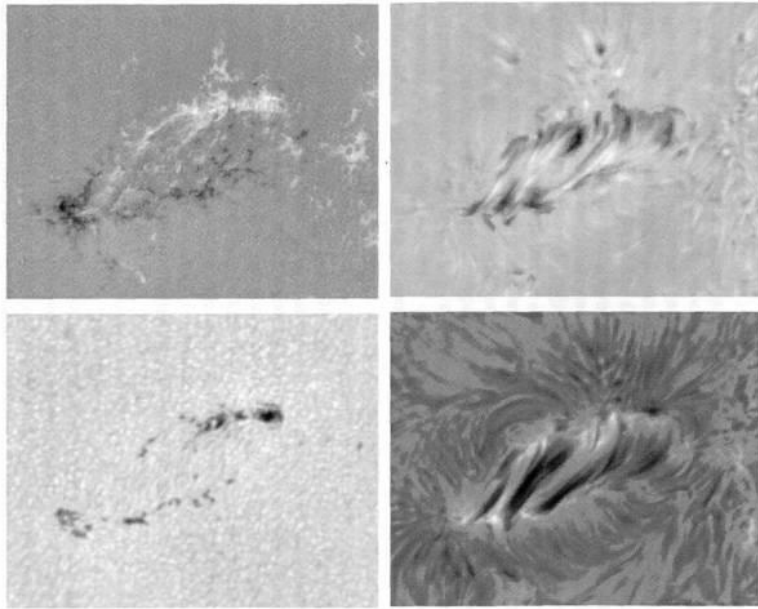


Fig. 1.6: Multi-band observations of an Arch Filament System. Top left: magnetogram created with the Zeeman Doppler Imaging technique; top right: Doppler-shift map, bottom left: continuum map; bottom right: H α image. Courtesy of Strous et al. 1996.

the growth of active regions, as Fig 1.6 showing an emerging active region viewed from different “bands”.

Plages are also prominently observed in the absorption lines Ca II K at 3933.67 \AA in the violet. Since it is the strongest solar spectral line observed from the ground, and that the plages make up about half of the Sun’s total magnetic flux (e.g. [124]), Ca II K lines are of great importance to the measurement of solar magnetic activities [49]. In fact, a strong correlation has been found between the Ca II K emission index and the sunspot number [19]; high correlation has also been emphasized between the plage area and the sunspot area in the yearly averaged data from 1907 to 1965 [83]. The century-long distribution of Ca II K from 1907 to 2007 saw an evolution of 11-year cycle in the butterfly diagram comparable to the sunspot butterfly diagram [33] (Fig. 1.4 vs Fig. 1.7). All sorts of evidence suggest, that magnetic field, produced by the dynamo in the convection zone, is the driving factor that brings about these observable solar activity features above.

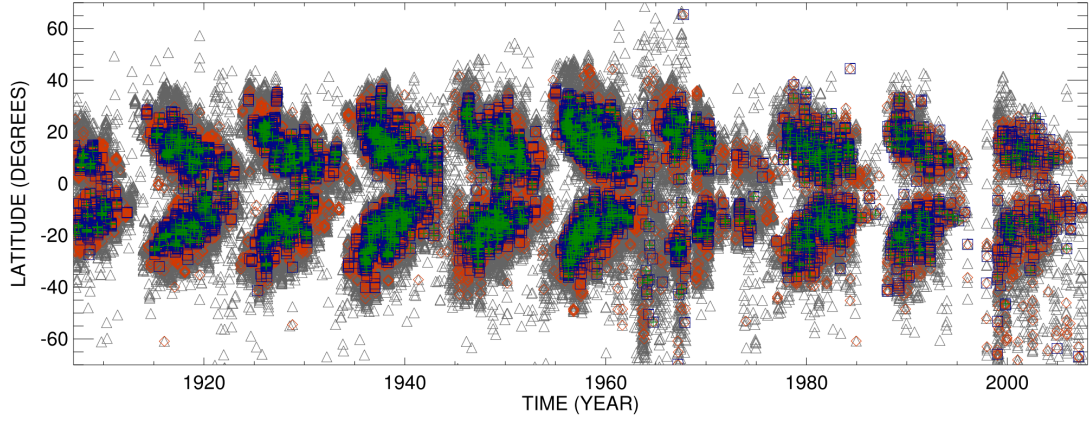


Fig. 1.7: Ca II K butterfly diagram. The gray triangles, red diamonds, blue squares, and green crosses depict centroids of plages with areas $\geq 1 \text{ arcmin}^2$, $\geq 4 \text{ arcmin}^2$, $\geq 7 \text{ arcmin}^2$ and $\geq 10 \text{ arcmin}^2$, respectively. Image courtesy of Kodaikanal Solar Observatory (KSO).

1.2.5 Granulation

Granulation is characterized by continually evolving cellular structures covering the entire solar photosphere except where sunspots lie, ranging from granules (a few Mm across for minutes) and mesogranules (5-10 Mm across for hours) to supergranules (20-50 Mm across for days). They are the direct observable evidence of convection below the solar surface. Generally speaking, bubbles of hotter gas from the convection zone rise upwards, appearing as brighter areas, and then cool down and sink inwards along the narrow darker intergranular lanes. Such convection patterns can be easily recognized in the hot Miso soup, or in the demonstration of heating silicone oil mixed with aluminium powder⁸. Granulations are driven by the dynamics throughout the convection zone. A review of the interplay between such dynamics and the magnetic fields will be laid out in § 1.2.8.

1.2.6 Flares

Solar flares are abrupt release of intense energy as a result of reconnecting magnetic fields especially in the sunspot groups. Observationally, they are seen as emission brightening with timescales ranging from minutes to hours. They can be seen at all wavelengths,

⁸Video available on Youtube: <https://www.youtube.com/watch?v=6w8u9YzZXNM>

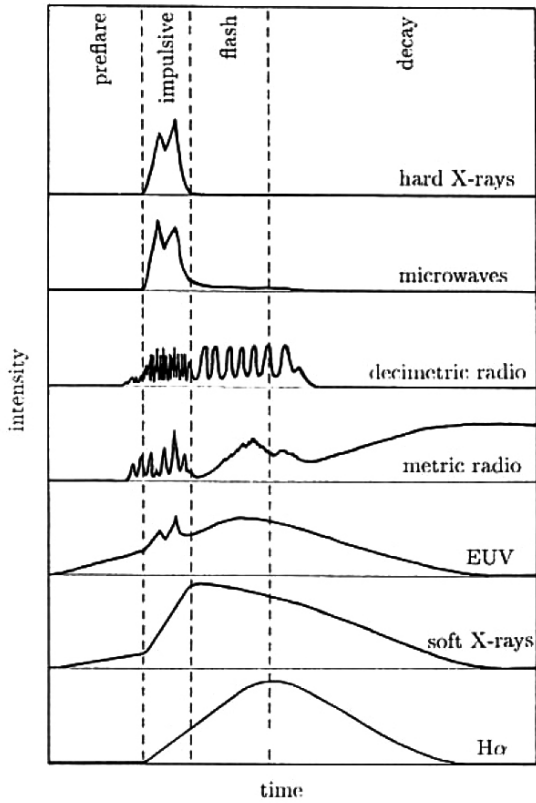


Fig. 1.8: Schematic profile of flare intensity in multiple wavelengths ([16], copy-right by Kluwer).

as shown in Fig. 1.8, including (a) soft X-rays and extreme ultraviolet (EUV) in the *preflare phase*, when the coronal plasma slowly heats up, (b) hard X-rays in the *impulsive phase*, when electrons and ions are energetically accelerated, (c) intensive radio emission produced by trapped high-energy particles in the *flash phase*, also characterized by soft X-ray and H α emissions, and (d) metrewave radio bursts caused by accelerated particles in the high corona, followed by the return of coronal plasma to its original state in the *decay phase* [17]. Solar flares differ from **solar prominences** in the sense that flares are eruptions of energy that have far-reaching effects, reaching even the earth in the form of electromagnetic radiation, whereas prominences either are self-contained arcs of ionized gas held by magnetic loops, typically extending to thousands of kilometres, or become active and eject gas away from the sun (Fig. 1.2).

1.2.7 Stellar Oscillations

Stellar oscillations or pulsations refer to the expansion and contraction of the stellar envelope. Pressure waves (or p-modes), generated by turbulent fluctuation in the convection zone, are refracted in the stellar interior and bounced back from the stellar surface, where density and pressure decrease rapidly. These trapped pressure waves can be described using spherical harmonics, and appear in multiple resonant modes in various frequencies.

Doppler imaging of the Sun shows signals that are strongest near the central stellar disk and weakest near the edge, indicating the oscillations take place mostly radially. Typical periods of individual p-mode oscillations for solar-like stars are a few minutes, with amplitudes of tens of cm s^{-1} ([24], [69]), however, the superimposed amplitude reach a few m s^{-1} .

Although stellar oscillations introduce noise to radial velocity observations, they reveal invaluable information on the stellar internal if treated properly. Helioseismology and asteroseismology have been powerful tools in studying the interiors of the Sun and other stars. The small intrinsic brightness variations due to p-modes in stars provide a rich spectrum of pulsation frequencies, and can determine the stellar mass, radius, age, chemical composition, etc. with unprecedentedly high precision ([129], [15], [74]). Moreover, helioseismology and asteroseismology have been successfully employed to probe the rotation and differential rotation of the Sun and solar-like stars ([1], [94], [93]). These “solar-like” p-mode oscillations can also be found in low-mass main sequence stars, massive main sequence stars and red-giant stars, as discovered by the French-led *COnvection ROtation and planetary Transits* (CoRoT) mission ([36], [38]) and NASA’s *Kepler* mission [31].

1.2.8 Solar Surface Magneto-Convection

Condition of convection Convection will take place if the condition of convection is met: a small volume of gas (or “bubble”) in temperature and pressure equilibrium with the surroundings becomes hotter than the surroundings when it rapidly rises under

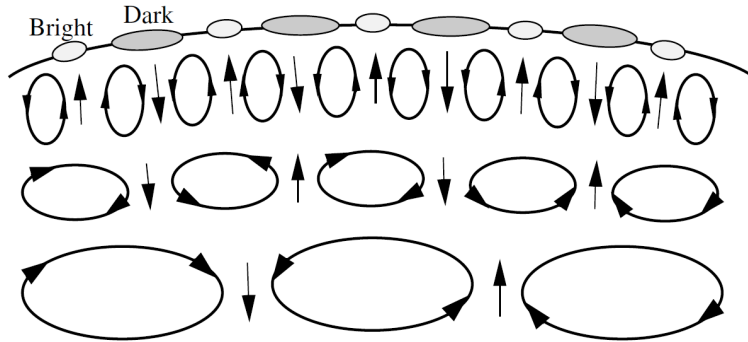


Fig. 1.9: Sketch of convective hierarchy in the sun [26].

perturbation. In other words, the radiative temperature gradient of the environment must be smaller than the adiabatic temperature gradient experienced by the bubble: $|dT/dr|_{\text{rad}} > |dT/dr|_{\text{adiab}}$.

Topology of convection Once convection is triggered, hotter gas rises due to buoyancy. As density and temperature decreases outwards in the stratified atmosphere, the gas exerts pressure on the surroundings and expand, giving upflows a tendency to diverge. It will then reach a point where the rising gas cools down via radiation and exchanging heat with the environment, turns over and is entrained in the surrounding downflow lanes. This is what happens for granulation at the top of the convection zone (§ 1.2.5).

Hierarchical structure of convection During convection, hotter gas is accelerated upwards while it diverges and tends to be laminar, whereas cooler gas is decelerated downwards while it converges and tends to be turbulent. Mass conservation is maintained [127]. Going inward, temperature increases in the convection zone, resulting in an increase of scale height. As a consequence, the sizes of convection cells, being proportional to the scale height, will increase if we go deeper into the convection zone [128].

Fig. 1.9 sketches the hierarchical structure of the solar convection zone.

Magnetic fields come into play We divide the discussion into two scenarios: (a) weak magnetic fields and (b) strong magnetic fields. The field strength is a relative concept regarding the magnetic energy compared with the kinetic energy of convection.

When magnetic field strength is weak, magnetic field lines are dragged by diverging upflows and swept into the intergranular lanes. The fields tend to be collected into the boundaries of granules, mesogranules, and supergranules in their corresponding granulation time-scales, producing a hierarchical structure of magnetic loops on different scales [128]. They are then stretched, twisted and intensified as a result of the down-flowing turbulence, where dynamo action takes place ([95], [135]).

When magnetic field strength is strong, convection is largely influenced by the Lorentz force $\mathbf{F} = q\mathbf{v} \times \mathbf{B}$, which acts perpendicularly to the direction of the magnetic field and inhibits convection in this direction. For example, strong magnetic fields which tend to be vertical [37] suppress the overturning flow of gas, a fundamental part of convection. Therefore, less energy is brought up to the surface via mass transportation and this area becomes cooler than the surroundings. This is the mechanism for forming sunspots and starspots (§ 1.2.2).

It is the interplay between the convective motion of gas and the magnetic fields that makes their behaviours complicated. In fact, magnetic features appear from unobservably small scales to hundreds of megameters [128]. It is found that they present a scale-free magnetogram distribution, suggesting either all scales of magnetic features are driven by the same mechanism (e.g. a scale-free dynamo acts throughout the convection zone), or some surface process dominates such a distribution in a scale-free way ([100], [132]). Further understanding of the magneto-convection relies on numerical recipes that treat plasma either fully ionized in an ideal manner or partially ionized in a realistic manner, which seeks to reveal the physics of magneto-convection related features like turbulent convection, dynamo action, flux emergence, sunspots, etc. [128].

1.3 The Challenge of Finding Exoplanets in the Presence of Stellar Noise

When it comes to detecting exoplanets, there is a “rivalry” between the amplitudes of exoplanet signals and stellar noise (often referred to as “jitter”), both of which produce radial velocity shifts. More massive and close-in planets are likely to stand out in the ocean of stellar noise; less massive and more distant planets are less easily discernible, even with every effort made to improve instrumentation precision. As such, periodic stellar jitter can lead to false detections ([23], [119]). In this section, we discuss the challenges for finding exoplanets in the presence of stellar noise and briefly present methods that aim to disentangle exoplanet signals from stellar noise.

1.3.1 The Amplitudes and Time-scales of Stellar Jitter

A variety of processes that can produce jitter were presented in § 1.2. Here we will look more closely at their radial velocity impacts, categorized by the time-scale over which they operate.

Minutes: stellar oscillations For GKM stars, Doppler radial velocity variations due to P-mode oscillations are at the order of m s^{-1} on time-scales less than 15 minutes (e.g. μ Arae, Fig. 1.10 (b), (c)). It has been shown that the oscillation frequencies

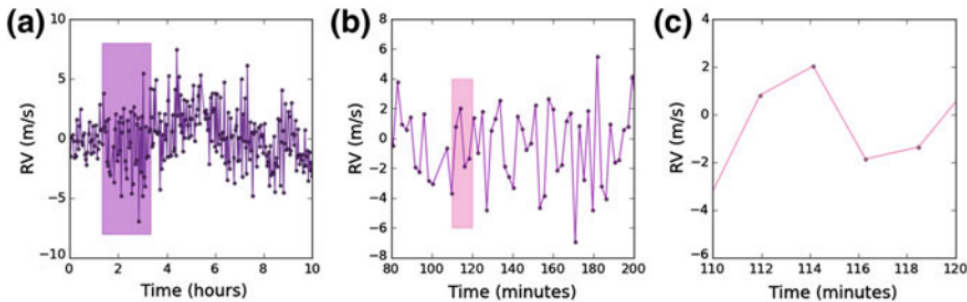


Fig. 1.10: Radial velocity observation of μ Arae (HD 160691), a bright Sun-like star. Panel (a) shows the stellar oscillation signals superimposed onto granulation signals. Panels (b) and (c) are zoom-ins of the previous panel, highlighting short-term oscillation signals. Data retrieved by [65] from [25].

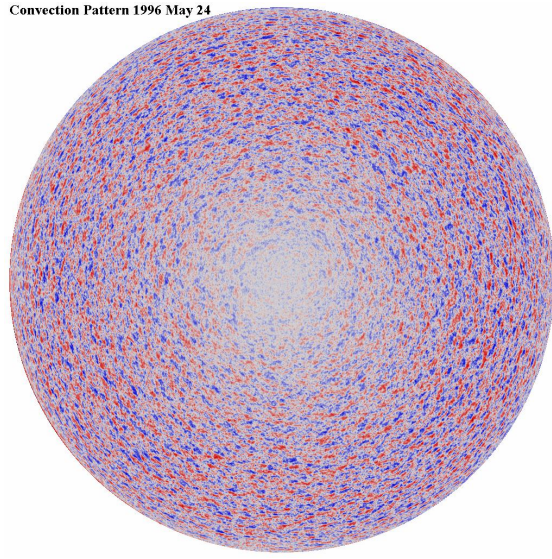


Fig. 1.11: Magnetic Doppler Imaging (MDI) data of the Sun, showing the supergranulation convection pattern. Red and blue colours are representations of redshift and blueshift. Image taken from Solar and Heliospheric Observatory (SOHO).

of p-modes are proportional to the square root of mean stellar density $\sqrt{\rho_{\text{star}}}$, and the radial velocity variation amplitudes are proportional to the luminosity-to-mass ratio L/M of the star [34]. As a result, oscillation periods and amplitudes become smaller for later spectral-types and for non-evolved stars, which tend to be denser and have lower luminosity-to-mass ratios. Observing these types of stars is therefore less affected by stellar oscillations, and so requires shorter exposure times (typically 1-2 oscillation periods) to average out oscillation impacts.

Minutes to hours: granulation Granulation produces a net blueshift of stellar spectra due to the convective upflows being hot and bright, whereas the downflows being cool and dark. Typical lifetimes for individual granulations range from minutes for granules, to hours for supergranules. Their overall radial velocity impact is a few m s^{-1} (e.g. μ Arae, Fig. 1.10 (a)), even though individual movements can reach up to a few km s^{-1} for granules and supergranules. Fig. 1.11 shows the radial velocity field of the Sun as a result of supergranules.

In the pursuit of sub- m s^{-1} precision, granulation remains a significant source of noise even if integrating over the stellar disc. One approach to reduce granulation jitter

is to take several observations of a star spanning across the same night and then bin the data, as to further average out fluctuations over the granulation time-scale [42].

Minutes to hours: flares Flares can impact planet searches around active M-dwarfs [106]. Common flares induce a radial velocity amplitude of $\sim 0.5 \text{ m s}^{-1}$ [121]. They last from minutes to hours, depending on the wavelengths of observation (§ 1.2.6, Fig. 1.2). For the Sun, the occurrence of flares follows the 11-year solar cycle; for M-dwarfs, however, flares can be non-periodic and more frequent [12]. To account for flare impact on radial velocities, equivalent width data for H α can be examined. H α emission is very sensitive to the presence of flares, and its variation can be used as a proxy for flare activity. [112] has shown a clear correlation between the flare-induced radial velocity shift and H α emission. It is worth noting that H α emission is not a measure which allows the impact of a flare to be calibrated out or removed, but it does allow individual exposures impacted by a flare to be discarded. The flares are so obviously identified that they do not actually pose danger to radial velocity surveys. Some M-dwarfs can be extremely quiet, however, as presented in the HARPS M-dwarf sample [22].

Days: starspots, faculae, plages Unlike stellar oscillations and granulations whose radial velocity impacts can be reduced by increasing exposure time or binning multiple observations to average over the typical time-scale of the variation, starspots are local dark features that appear in the stellar rotation period on time-scales of days, and on which themselves come and go on the time-scale of the much longer stellar magnetic cycle (\sim years). Starspots break the brightness symmetry of the stellar disc. So as stars rotate, a starspot moving towards (Fig. 1.12, 2nd panel) / away (Fig. 1.12, 4th panel) from us will redshift / blueshift the net spectrum by distorting the spectral line profile. The amplitudes of such Doppler shifts will depend on how fast the star rotates, and the temperature, sizes and distribution of starspots, but generally fall in the order of 1 m s^{-1} ([73], [82]). Faculae and plages have similar impacts, with the difference that they are features of enhanced surface brightness.

A second factor affecting radial velocity measurements is the inhibition of convective blueshift (as discussed in the granulation paragraphs above) in the starspot regions,

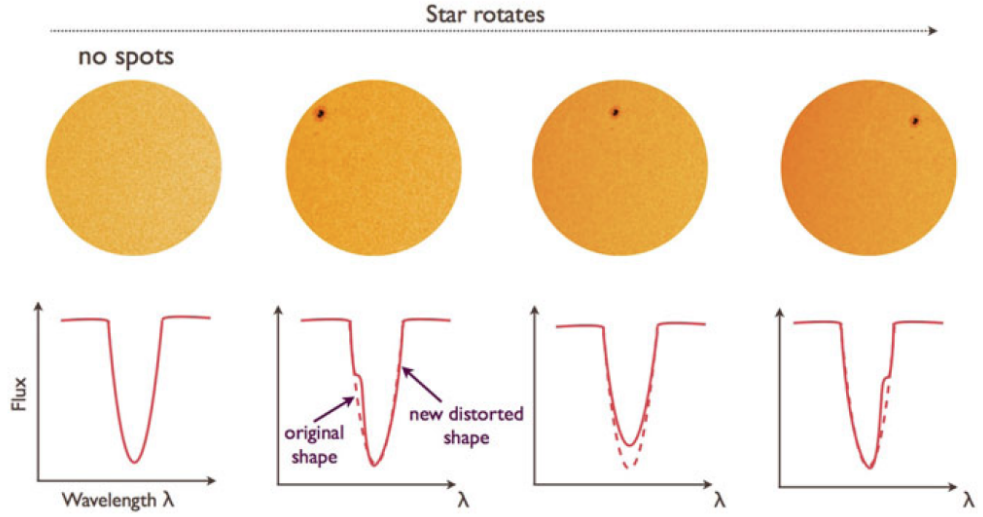


Fig. 1.12: Dark spot → flux imbalance on stellar disc → spectral line asymmetry → radial velocity variation.

where strong magnetic fields suppress convection (refer to § 1.2.8). It appears as a time-dependent redshift relative to the approximately non-time-evolving convective blueshift.

For rapidly rotating stars, the impacts of starspots dominate over the inhibition of blueshift convection, as radial velocity variations due to starspots are proportional to the projected radial velocity of the rotation of stars $v \sin i$; for slowly rotating stars, the inhibition of convective blueshift can dominate over starspots [106]. Based on “Sun as a planet-host star” observations acquired with the Solar Dynamics Observatory (SDO), [66] has reported that the radial velocity variation from inhibition of convective blueshift has an amplitude of 2.40 m s^{-1} , whereas that from the flux imbalance due to sunspots, faculae and plages has an amplitude of 0.41 m s^{-1} .

Decades: magnetic cycles As was discussed in § 1.2, starspots, faculae, plages, flares, etc. are consequences of stellar magnetic activity, and will have impacts that vary on the stellar rotation period on timescales of days. These activity signatures are superimposed onto magnetic cycles of a few years exhibited in Sun-like stars. As such, there are two aspects of radial velocity jitter presented: (a) its short-term scatter will become larger at activity-maximum and lower at activity-minimum, and (b) it may produce a systematic radial velocity trend over the magnetic activity cycle, as the

radial velocities are affected by the fraction of stellar disc, covered by spots, faculae and plages, which suppress convective blueshift. Therefore, observing stars at their activity-minimum stage will minimize stellar jitter effects on planet-induced radial velocities. Simultaneous analysis of activity indexes (e.g. S_{HK} and $\log R'_{HK}$ from Ca II H&K lines; refer to § 1.3.4) over the long baseline observations is necessary to rule out the possibility of stellar activities mimicking planetary signals ([67], [44]).

The magnitudes of magnetic activity depend on stellar age. Generally speaking, searching planets around young stars ($\lesssim 1$ Gyr) is very difficult. Starspots alone can cause radial velocity jitter over tens of m s^{-1} , making the detection of even hot Jupiters unlikely. They are certainly not the targets of our prior interest in the search of exoplanet as potential host for extraterrestrial intelligence, considering the timescale to form civilization in our solar system. Stars like our Sun is not as active in comparison. Sun-like stars steadily slow down and their magnetic dynamo weakens with age ([137], [96]). Their rotation period increases from $\sim 1\text{-}2$ days at 5 Myr to 20-50 days at 5 Gyr, and thus the stellar jitter is expected to be reduced. About 10-20% old Sun-like stars are nearly inactive and do not show cyclic variations [79].

(I may discuss the magnetic activity dependence on spectral type in the future.)

Varying time-scale: gravitational redshift Gravitational redshift is a recently identified source of stellar jitter, arising from stellar radius fluctuations. It is believed a 0.01% change of solar radius would produce 6 cm gravitational redshift, possibly obstructing detecting Earth-twins. A few sources of gravitational redshift were presented by [30], indicating it is at the order of a few cm s^{-1} and may be non-negligible in search of low-mass terrestrial planets:

- **Magnetic activity:** The impacts of stellar radius fluctuations due to both Applegate effect (i.e. magnetic activity cycle causes stellar radius fluctuations through changing the stellar gravitational quadrupole moment and altering the oblateness of the star [8]) and inhibition of convection demonstrate a few cm s^{-1} radial velocity variations.

- **Wilson depression of starspots:** Wilson depression ([138], [92]) refers to the funnel shape of starspots, which physically decreases the local radius. For quiet solar-like stars, such an effect is estimated to be a few cm s^{-1} on radial velocities.
- **Stellar oscillations:** The characteristic time-scale of radius fluctuation at which gravitational redshift become dominant over Doppler redshift is proportional to R^2/M , where R is the stellar radius and M is the stellar mass. This is ~ 10 days for low-mass stars, for which stellar oscillation is not a concern considering its short time-scale. However, the gravitational redshift may become considerable for evolved stars.

Varying time-scale: binary companions While double-lined spectroscopic binaries are easy to identify, more often than not, the other companion is either too faint to be observed or too close to be resolved through spectrographs. As a result, it can be difficult to rule out stellar companions from exoplanet signatures, as in the case of HD 41004, where a 1.3-day period, 50 m s^{-1} radial velocity amplitude brown dwarf was disguised as a planet orbiting an M dwarf with a K dwarf companion ([142], [122]). [88] has shown that a tight binary system orbiting another star mimics the presence of two planets with similar orbital periods.

1.3.2 The Properties of Stars as a Function of Spectral Type

The key to precise radial velocity measurement lies in determining the centroid of the spectral line profile. It is intuitive that (a) the narrower and deeper a line is, the more constrained is its centroid, and (b) the higher signal-to-noise ratio of an observation, the better defined of a line profile. For a Gaussian shape line profile approximation, it can be shown that [79]

$$\sigma_{\text{RV}} \sim \frac{\sqrt{\text{FWHM}}}{C \cdot \text{SNR}} \quad (1.2)$$

where the centroid uncertainty of a Gaussian line profile σ_{RV} can be expressed as a function of its full width at half-maximum (FWHM), contrast (i.e. depth relative to continuum) C and signal-to-noise ratio (SNR). Expression (1.2) can be further simplified by

introducing a constraint between full width at half-maximum and depth: $C \sim 1/\text{FWHM}$, so that

$$\sigma_{\text{RV}} \sim \frac{\text{FWHM}^{3/2}}{\text{SNR}} \propto \text{FWHM}^{3/2}. \quad (1.3)$$

For example, a reduction of FWHM by half is estimated to reduce (i.e. improve) σ_{RV} by two thirds. This is why Doppler programmes tend to concentrate on slowly rotating stars using high resolution spectrographs to achieve high radial velocity precision. So stars are advantaged or disadvantaged for high precision radial velocities by their spectral type:

Hot stars Stars hotter than 10,000 K are unfavourable, as spectral lines are hardly present due to high levels of ionization. Moreover, hot stars tend to be young and fast rotating, which flattens out any existing spectral lines due to rotational broadening.

Red giants Probing red giant branch stars and red clump giants provides an alternative means to observe intermediate-mass stars, despite them being active and rapidly rotating in their early evolution stage. These stars become sufficiently cool and spin down, and present large amount of narrow spectral line features when they evolve into giants. However, the radial velocities are more susceptible to stellar pulsations, which are stronger in low gravity stars.

F5 to M5 stars Stars from F5 to M5, corresponding to masses between $\sim 1.5M_{\odot}$ and $\sim 0.1M_{\odot}$, are favourable for Doppler planet detections: (a) planets produce larger radial velocity wobbles than orbiting a less massive star, and (b) thousands of absorption lines, essential for precise radial velocity observations, are present in the visible and near-infrared regions. For FGK stars, Fe lines are the most abundant.

Cool stars Stars cooler than 3,500 K have the advantage that their spectrum is composed of millions of molecular absorption lines, but the disadvantage that those lines are significantly overlapping. The fact that most of their flux are emitted in the infrared poses a great challenge for ground-based telescopes. Even though early M

dwarfs (M0 to M4) are bright enough in the solar neighbourhood, they are more active than FGK stars in general.

1.3.3 Two Components of Radial Velocity Shifts

There are two factors that can change the centroid of a spectral line. The Keplerian motion of gravitationally bound companions (including planets), which result in the corresponding reflex motion of the parent star, producing a Doppler shift of the stellar spectrum. This component does not change the shape of the spectral line profile. It is also achromatic, producing exactly the same effects at all wavelengths. This is the centroid shift we seek to measure in the radial velocity search of exoplanets. The other factor is flux imbalance on the surface of the star, resulting in an asymmetric change to the emergent line profile in the stellar spectrum. It changes the shape of the spectrum and produces radial velocity noise in the search for exoplanets (e.g. Fig. 1.12). We therefore write the observed radial velocity shift v_{obs} as the sum of planet-induced radial velocity v_p and activity-induced radial velocity v_a :

$$v_{\text{obs}} = v_p + v_a. \quad (1.4)$$

The scope of this thesis aims to quantitatively determine v_a , the intrinsic stellar variability, as a correction term.

1.3.4 Observational Methods for Detection and Quantification of Stellar Activity

Cross correlation function The cross correlation function (CCF) of the spectrum is often used to represent a high signal-to-noise ratio averaged line profile (e.g. [107], [14], [79]). It is obtained by cross-correlating the observed spectrum with the stellar template. Ideally, a template spectrum requires very high signal-to-noise ratio for each target star, which is however very observationally demanding. One treatment is to co-add all the observations of the same target to obtain the template with enhanced signal-to-noise ratio, which requires a large number of observations. Another treatment

is to use a “box” function (i.e. a binary function of 1’s at the positions of spectral lines and 0’s elsewhere) as a mask, against which the observed spectrum is cross-correlated with. This simply requires a priori knowledge of the line positions for the particular type of star being observed. The “box” function template is weighted by the contrast of the line (same as the contrast in Eq. 1.2), as higher contrast means more radial velocity information). So overall, the cross correlation function represents a weighted average of all the lines presented in the target star.

Measure of spectral line profile deformation The full width at half-maximum (FWHM) and bisector of the cross correlation function have often been used as a quantitative proxy to probe for the presence and strength of stellar activity.

- **Full width at half-maximum** of the cross correlation function measures the broadening of spectral lines. Activity features such as starspots, plages and faculae produce imbalanced flux on the stellar disc and therefore break the symmetry of the spectral lines, which can be observed in the full width at half-maximum of the line profile, through seeking periodic signals in the variation of full width at half-maximum at the stellar rotation period ([108], [64]).
- The line “**bisector**” is defined as the mid point of a line profile (or equivalently of a cross correlation function) - it divides the line profile into halves of equal width as a function of line depth [102]. It can be used to describe the asymmetry of a line profile, inasmuch as a symmetric profile produces a vertical bisector - deviations from a vertical bisector are a signature of line asymmetry. Various versions of bisector analysis can be found in the literature (Fig. 1.13), such as (a) the *bisector velocity span*, defined as the different bisector velocity at the top and at the bottom of the line profile $v_t - v_b$, an indication the bisector’s first derivative [133] (or equivalently the *bisector inverse slope*, defined as the inverse of the mean slope of the bisector [109]), (b) the *bisector curvature*, defined as the velocity span between the midpoint on the bisector and centre of the end points, which is an indication the bisector’s second derivative ([63], [57]), and (c) the *bi-Gaussian*, which is characterized by fitting each half of the line profile

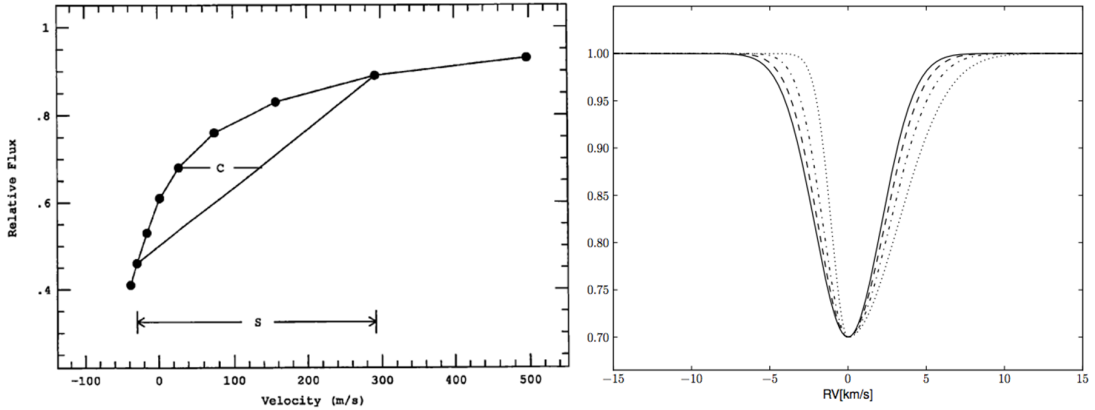


Fig. 1.13: Various ways to quantify the bisector of a spectral line profile. Left panel: s is the bisector velocity span and c represents the bisector curvature [63]. Right panel: line profiles from left to right are of 0%, 10%, 25% and 50% asymmetry. The percentage is associated with the full widths at half maximum of the fitted bi-Gaussian [47].

with Gaussian functions of different half width at half maximum ([47], [91]). The correlation between bisector span and activity-induced radial velocity has been implemented to correct stellar jitter (e.g. [87], [21]), however, [20] argues that the degree of correlation depends on the spot configuration, latitude and stellar rotation $v \sin i$, and the correlation is not always present.

Activity indicators from spectral lines In addition to looking at the whole spectrum, there are other indexes based on particular spectral lines that sensitively respond to stellar activity, as outlined below:

- **Ca II H and K doublet:** The core emission of calcium II H and K absorption lines at 3968.5Å and 3933.7Å is known to correlate with stellar chromospheric ([11], [77]) and long term magnetic cycles (e.g. [60], [104], Ca II K butterfly diagram in Fig. 1.7 and periodic S-index of the Sun observed by Mount Wilson Observatory [43]). The S-index and R'_{HK} index have been introduced to quantify the strength of core emission of calcium H and K doublet.

- **S-index** was first used by Mount Wilson Observatory as a magnetic activity proxy [134]:

$$S = \alpha \frac{N_H + N_K}{N_R + N_V} \quad (1.5)$$

where N_H and N_K are the flux counts in the core of H and K lines, N_R and N_V are the counts in the adjacent continuum (red and violet), and α is a calibration constant. Although S-index is widely used as an activity indicator, it is spectral-type and instrument dependent, which restrains its use when comparing among stars and observations [65].

- The **R'_{HK}** index was first introduced to overcome the S-index's dependence on spectral-type and instrumental design [96]. It is defined as the chromospheric contribution (in which the photospheric component needs to be subtracted) of calcium H and K lines normalized by the bolometric brightness of the star:

$$R'_{HK} = \frac{F'_H + F'_K}{\sigma T_{\text{eff}}^4}. \quad (1.6)$$

In practice, $\log R'_{HK}$ is often used. It ranges from about -4.4 for highly active stars to -5.1 for very inactive stars [59]. R'_{HK} is widely adopted as an indicator for stellar chromospheric variability, so searches for periodic variability in this index can be used to reject false planetary signals at that period ([108], [81], [130]). It has also been found that R'_{HK} linearly correlates with the rotation period in logarithmic scale for low mass stars ([131], [10]). Because of this, it can be used to estimate the rotation period of low-mass stars from $\log R'_{HK}$.

Their location in the violet region of the optical spectrum means that the calcium II H and K doublet becomes less useful for cool stars, because the energy distribution of the spectrum of cool stars is shifted to longer wavelengths. It results in low signal-to-noise ratios of the Ca II H and K lines and limit their use for cool stars.

- **H α :** Activity as measured via core emission in the H α line at 6562.8Å has, for a long time, been believed to be tightly correlated the core emission in the Ca II H and K doublet. As a result, they have been used interchangeably as chromospheric activity indicators (e.g. [115], [118], [62]). Recent studies, however, have

indicated this picture may not be as simple as previously assumed, with a variety of correlation coefficients between these two indexes observed - potentially arising from the different contributions of filaments and plages to calcium II doublets and H α (see e.g. [35], [55], [116]). It has also been argued that H α is less sensitive than calcium H and K doublets in measuring long-term activities [54].

In spite of this, located in the visible red region, H α is a much more readily observable indicator for cool stars. It is often used in combination with other activity indicators to test whether exoplanet candidates could be caused by stellar activity (e.g. Gliese 581: [118]; debate on the Kapteyn's star: [119], [7]). In addition, H α emission studies of active M dwarfs ([27], [113]) have led to consistent results for a rotation-activity relation - stars with higher rotational velocities are more active up until this correlation saturates at a stellar-mass dependent threshold velocity [105]. However, it should be noted that frequent flare events in active M dwarfs can induce a large scatter of H α index.

- **Sodium D lines:** The Sodium D₁ and D₂ doublet show emission in the core in response to chromospheric activities. As for H α , the Sodium D lines (at 5895.92Å and 5889.95Å in the yellow region of the optical spectrum) are prominent features that outperform the Ca II H and K doublet as a predictor of radial velocity jitter in cool stars like M dwarfs [55]. The sodium D lines diagnose activity information in the middle-to-lower chromosphere for M dwarfs, as opposed to H α which probes the upper chromosphere and lower transition region ([4], [84]), and thus can be used as a complementary activity indicator to H α . Sodium D lines have been used to look at stellar variability, such as the cases of GJ 176 [117], Gliese 581 [118] and several other M dwarfs in [56].

Photometry Photometry provides a probe into stellar activity signals in two ways. (1) Analogous to the activity indicators discussed above, intrinsic variations of photometry imply the presence of stellar surface inhomogeneity due to stellar activity ([72], [18]). Caution must be taken when the photometric period is close to the orbital period of a planet candidate. (2) Derived from a spot model, the stellar photometric and activity-induced radial velocity variations can be linked, which can be used as a correction term

to reduce the root mean square (rms) of the radial velocity residual [2]. However, the absence of photometric variability does not necessarily imply an inactive star, as photometry is largely insensitive to stellar faculae, and some active regions present radial velocity signals rather than photometric signals [3].

Lomb-Scargle periodogram The *Lomb-Scargle periodogram* (LS) is perhaps the most widely used tool in analysing radial velocity data in the search of exoplanets. It plays an important role in determining (a) the orbital periods of planets, (b) the periodicity of stellar activity signals and (c) whether stellar activity signals mimic planetary signals. Apart from Doppler detections of exoplanets, the Lomb-Scargle periodogram is also good at mining periodic signals, such as stellar oscillation, granulation, planet transiting light curves, etc.

This method was first proposed by Lomb [78] and Scargle [123], and later developed by Zechmeister and Küster [141] as the *generalized Lomb-Scargle periodogram* (GLS). The basic idea is fitting the radial velocity data set y_i observed at times t_i with error σ_i by a linear combination of sinusoids with an offset C

$$y(t_i) = A \cos(\omega t_i) + B \sin(\omega t_i) + C, \quad (1.7)$$

and minimizing the difference between the model $y(t_i)$ and the data y_i

$$\chi^2 = \sum_{n=1}^N \frac{[y(t_i) - y_i]^2}{\sigma_i^2}. \quad (1.8)$$

It enables a power spectrum in frequency space $p(\omega)$ to be calculated to indicate the goodness of the fit given a particular frequency. The generalized Lomb-Scargle periodogram was designed to model the power spectrum produced by circular orbits, but an algorithm has also been given to allow for the detection of eccentric Keplerian orbits, which is similar to the *two dimensional Kepler Lomb-Scargle periodogram* (2DKLS) developed in [99] and [98], to better cope with uneven sampling and noise. Recently, the stacked Bayesian general Lomb-Scargle periodogram has been introduced to rule out

unstable and incoherent signals, such as stellar activity, by stacking the periodogram and tracking the power spectrum over time [89].

1.3.5 Summary

The challenge of finding exoplanets with radial velocity methods lies in disentangling planetary signals from stellar jitter which has both comparable amplitudes and time-scales. It requires a detailed understanding of the impact of stellar activity, which is however limited, since our knowledge of stellar features have been largely built upon observations of our Sun. High resolution spectroscopy allows us to detect radial velocities of distant stars at high precision. However, to detect low-amplitude exoplanetary signals, we must develop tools to correct for activity-induced radial velocity signals. Individual or combined activity indexes, derived from the spectral line profile, can be used to trace the rotation period of the star and introduced as a radial velocity correction term. No indicator, to date, however, has proven universally applicable. This thesis will further quantify how line profile deformation caused by stellar activity can impact radial velocity detections of exoplanet.

1.4 References

- [1] C. Aerts. The age and interior rotation of stars from asteroseismology. *Astronomische Nachrichten*, 336(5):477–486, 2015. 17
- [2] S. Aigrain, F. Pont, and S. Zucker. A simple method to estimate radial velocity variations due to stellar activity using photometry. , 419:3147–3158, February 2012. 32
- [3] Aigrain, S., Angus, R., Barstow, J., Rajpaul, V., Gillen, E., Parviainen, H., Pope, B., Roberts, S., McQuillan, A., Gibson, N., Mazeh, T., Pont, F., and Zucker, S. The effects of stellar activity on detecting and characterising exoplanets. 2016. 32
- [4] V. Andretta, J. G. Doyle, and P. B. Byrne. The NaI $\lambda\lambda 5890, 5896$ resonance doublet as chromospheric diagnostics in M dwarfs. , 322:266–279, June 1997. 31
- [5] G. Anglada-Escudé, P. J. Amado, J. Barnes, Z. M. Berdiñas, R. P. Butler, G. A. L. Coleman, I. de La Cueva, S. Dreizler, M. Endl, B. Giesers, S. V. Jeffers, J. S. Jenkins, H. R. A. Jones, M. Kiraga, M. Kürster, M. J. López-González, C. J. Marvin, N. Morales, J. Morin, R. P. Nelson, J. L. Ortiz, A. Ofir, S.-J. Paardekooper, A. Reiners, E. Rodríguez, C. Rodríguez-López, L. F. Sarmiento, J. P. Strachan, Y. Tsapras, M. Tuomi, and M. Zechmeister. A terrestrial planet candidate in a temperate orbit around Proxima Centauri. , 536:437–440, August 2016. 4
- [6] G. Anglada-Escudé, P. Arriagada, S. S. Vogt, E. J. Rivera, R. P. Butler, J. D. Crane, S. A. Shectman, I. B. Thompson, D. Minniti, N. Haghjhipour, B. D. Carter, C. G. Tinney, R. A. Wittenmyer, J. A. Bailey, S. J. O’Toole, H. R. A. Jones, and J. S. Jenkins. A Planetary System around the nearby M Dwarf GJ 667C with At Least One Super-Earth in Its Habitable Zone. , 751:L16, May 2012. 7
- [7] G. Anglada-Escudé, M. Tuomi, P. Arriagada, M. Zechmeister, J. S. Jenkins, A. Ofir, S. Dreizler, E. Gerlach, C. J. Marvin, A. Reiners, S. V. Jeffers, R. Paul Butler, S. S. Vogt, P. J. Amado, C. Rodríguez-López, Z. M. Berdiñas, J. Morin, J. D. Crane, S. A. Shectman, M. R. Díaz, L. F. Sarmiento, and H. R. A. Jones. No evidence for activity correlations in the radial velocities of kapteyn’s star. *The Astrophysical Journal*, 830(2):74, 2016. 31
- [8] J. H. Applegate. A mechanism for orbital period modulation in close binaries. , 385:621–629, February 1992. 24
- [9] NASA Exoplanet Archive. Exoplanet detection by year. Available at <http://exoplanetarchive.ipac.caltech.edu/exoplanetplots/> (2017/02/14). 3
- [10] Astudillo-Defru, N., Delfosse, X., Bonfils, X., Forveille, T., Lovis, C., and Rameau, J. Magnetic activity in the harps m dwarf sample - the rotation-activity relationship for very low-mass stars through r’hk. *AA*, 600:A13, 2017. 30
- [11] R. G. Athay. A Non-Lte Line-Blanketed Solar Model. , 161:713, August 1970. 29

- [12] M. Audard, M. Güdel, J. J. Drake, and V. L. Kashyap. Extreme-Ultraviolet Flare Activity in Late-Type Stars. , 541:396–409, September 2000. 22
- [13] H. W. Babcock. The Topology of the Sun’s Magnetic Field and the 22-YEAR Cycle. , 133:572, March 1961. 10
- [14] A. Baranne, D. Queloz, M. Mayor, G. Adrianzyk, G. Knispel, D. Kohler, D. Lacroix, J.-P. Meunier, G. Rimbaud, and A. Vin. ELODIE: A spectrograph for accurate radial velocity measurements. , 119:373–390, October 1996. 27
- [15] Sarbani Basu, William J. Chaplin, and Yvonne Elsworth. Determination of stellar radii from asteroseismic data. *The Astrophysical Journal*, 710(2):1596, 2010. 17
- [16] A. Benz, editor. *Plasma Astrophysics, second edition*, volume 279 of *Astrophysics and Space Science Library*, June 2002. 16
- [17] Arnold O. Benz. Flare observations. *Living Reviews in Solar Physics*, 14(1):2, 2016. 16
- [18] Svetlana V. Berdyugina. Starspots: A key to the stellar dynamo. *Living Reviews in Solar Physics*, 2(1):8, 2005. 10, 31
- [19] Luca Bertello, Alexei Pevtsov, Andrey Tlatov, and Jagdev Singh. Correlation between sunspot number and ca ii k emission index. *Solar Physics*, 291(9):2967–2979, 2016. 14
- [20] Boisse, I., Bouchy, F., Hébrard, G., Bonfils, X., Santos, N., and Vauclair, S. Disentangling between stellar activity and planetary signals. *AA*, 528:A4, 2011. 29
- [21] Boisse, I., Moutou, C., Vidal-Madjar, A., Bouchy, F., Pont, F., Hébrard, G., Bonfils, X., Croll, B., Delfosse, X., Desort, M., Forveille, T., Lagrange, A.-M., Loeillet, B., Lovis, C., Matthews, J. M., Mayor, M., Pepe, F., Perrier, C., Queloz, D., Rowe, J. F., Santos, N. C., Ségransan, D., and Udry, S. Stellar activity of planetary host star hd189733. *AA*, 495(3):959–966, 2009. 29
- [22] X. Bonfils, X. Delfosse, S. Udry, T. Forveille, M. Mayor, C. Perrier, F. Bouchy, M. Gillon, C. Lovis, F. Pepe, D. Queloz, N. C. Santos, D. Ségransan, and J.-L. Bertaux. The HARPS search for southern extra-solar planets. XXXI. The M-dwarf sample. , 549:A109, January 2013. 22
- [23] X. Bonfils, M. Mayor, X. Delfosse, T. Forveille, M. Gillon, C. Perrier, S. Udry, F. Bouchy, C. Lovis, F. Pepe, D. Queloz, N. C. Santos, and J.-L. Bertaux. The HARPS search for southern extra-solar planets. X. A m sin i = 11 M_⊕planet around the nearby spotted M-dwarf <ASTROBJ> GJ674 </ASTROBJ>, 474 : 293 – 299, October 2007. 20
- [24] F. Bouchy and F. Carrier. P-mode observations on α Cen A. , 374:L5–L8, July 2001. 17

- [25] Bouchy, F., Bazot, M., Santos, N. C., Vauclair, S., and nowska, D. So. Asteroseismology of the planet-hosting star μ aerae - i. the acoustic spectrum. *AA*, 440(2):609–614, 2005. 20
- [26] H. Bradt. *Astrophysics Processes*. September 2008. 18
- [27] M. K. Browning, G. Basri, G. W. Marcy, A. A. West, and J. Zhang. Rotation and Magnetic Activity in a Sample of M-Dwarfs. , 139:504–518, February 2010. 31
- [28] R. P. Butler, G. W. Marcy, D. A. Fischer, T. M. Brown, A. R. Contos, S. G. Korzennik, P. Nisenson, and R. W. Noyes. Evidence for Multiple Companions to Andromedae. , 526:916–927, December 1999. 4
- [29] B. W. Carroll and D. A. Ostlie. *An introduction to modern astrophysics and cosmology*. July 2006. 13
- [30] H. M. Cegla, C. A. Watson, T. R. Marsh, S. Shelyag, V. Moulds, S. Littlefair, M. Mathioudakis, D. Pollacco, and X. Bonfils. Stellar jitter from variable gravitational redshift: implications for radial velocity confirmation of habitable exoplanets. , 421:L54–L58, March 2012. 24
- [31] W. J. Chaplin, H. Kjeldsen, J. Christensen-Dalsgaard, S. Basu, A. Miglio, T. Appourchaux, T. R. Bedding, Y. Elsworth, R. A. García, R. L. Gilliland, L. Giardini, G. Houdek, C. Karoff, S. D. Kawaler, T. S. Metcalfe, J. Molenda-Żakowicz, M. J. P. F. G. Monteiro, M. J. Thompson, G. A. Verner, J. Ballot, A. Bonanno, I. M. Brandão, A.-M. Broomhall, H. Bruntt, T. L. Campante, E. Corsaro, O. L. Creevey, G. Doğan, L. Esch, N. Gai, P. Gaulme, S. J. Hale, R. Handberg, S. Hekker, D. Huber, A. Jiménez, S. Mathur, A. Mazumdar, B. Mosser, R. New, M. H. Pinsonneault, D. Pricopi, P.-O. Quirion, C. Régulo, D. Salabert, A. M. Serenelli, V. Silva Aguirre, S. G. Sousa, D. Stello, I. R. Stevens, M. D. Suran, K. Uytterhoeven, T. R. White, W. J. Borucki, T. M. Brown, J. M. Jenkins, K. Kinemuchi, J. Van Cleve, and T. C. Klaus. Ensemble Asteroseismology of Solar-Type Stars with the NASA Kepler Mission. *Science*, 332:213, April 2011. 17
- [32] Paul Charbonneau. Dynamo models of the solar cycle. *Living Reviews in Solar Physics*, 2(1):2, 2005. 11
- [33] Subhamoy Chatterjee, Dipankar Banerjee, and B. Ravindra. A butterfly diagram and carrington maps for century-long ca ii k spectroheliograms from the kodaikanal observatory. *The Astrophysical Journal*, 827(1):87, 2016. 14
- [34] JØrgen Christensen-Dalsgaard. Physics of solar-like oscillations. *Solar Physics*, 220(2):137–168, 2004. 21
- [35] C. Cincunegui, R. F. Díaz, and P. J. D. Mauas. H α and the Ca II H and K lines as activity proxies for late-type stars. , 469:309–317, July 2007. 31
- [36] Joris De Ridder, Caroline Barban, Frederic Baudin, Fabien Carrier, Artie P. Hatzes, Saskia Hekker, Thomas Kallinger, Werner W. Weiss, Annie Baglin, Michel Auvergne, Reza Samadi, Pierre Barge, and Magali Deleuil. Non-radial oscillation modes with long lifetimes in giant stars. *Nature*, 459(7245):398–400, 05 2009. 17

- [37] A. G. de Wijn, J. O. Stenflo, S. K. Solanki, and S. Tsuneta. Small-scale solar magnetic fields. *Space Science Reviews*, 144(1):275, 2008. 19
- [38] M. P. Di Mauro. A review on Asteroseismology. *ArXiv e-prints*, March 2017. 17
- [39] J.-F. Donati, I. D. Howarth, M. M. Jardine, P. Petit, C. Catala, J. D. Landstreet, J.-C. Bouret, E. Alecian, J. R. Barnes, T. Forveille, F. Paletou, and N. Manset. The surprising magnetic topology of τ Sco: fossil remnant or dynamo output? , 370:629–644, August 2006. 12
- [40] X. Dumusque. Radial velocity fitting challenge. I. Simulating the data set including realistic stellar radial-velocity signals. , 593:A5, August 2016. 7, 8
- [41] X. Dumusque, F. Pepe, C. Lovis, D. Ségransan, J. Sahlmann, W. Benz, F. Bouchy, M. Mayor, D. Queloz, N. Santos, and S. Udry. An Earth-mass planet orbiting α Centauri B. , 491:207–211, November 2012. 7
- [42] Dumusque, X., Udry, S., Lovis, C., Santos, N. C., and Monteiro, M. J. P. F. G. Planetary detection limits taking into account stellar noise - i. observational strategies to reduce stellar oscillation and granulation effects. *AA*, 525:A140, 2011. 22
- [43] Ricky Egeland, Willie Soon, Sallie Baliunas, Jeffrey C. Hall, Alexei A. Pevtsov, and Luca Bertello. The mount wilson observatory s-index of the sun. *The Astrophysical Journal*, 835(1):25, 2017. 29
- [44] M. Endl, E. J. Brugamyer, W. D. Cochran, P. J. MacQueen, P. Robertson, S. Meschiari, I. Ramirez, M. Shetrone, K. Gullikson, M. C. Johnson, R. Wittenmyer, J. Horner, D. R. Ciardi, E. Horch, A. E. Simon, S. B. Howell, M. Everett, C. Caldwell, and B. G. Castanheira. Two New Long-period Giant Planets from the McDonald Observatory Planet Search and Two Stars with Long-period Radial Velocity Signals Related to Stellar Activity Cycles. , 818:34, February 2016. 24
- [45] Yuhong Fan. Magnetic fields in the solar convection zone. *Living Reviews in Solar Physics*, 6(1):4, 2009. 11
- [46] F. Feroz and M. P. Hobson. Bayesian analysis of radial velocity data of GJ667C with correlated noise: evidence for only two planets. , 437:3540–3549, February 2014. 7
- [47] P. Figueira, N. C. Santos, F. Pepe, C. Lovis, and N. Nardetto. Line-profile variations in radial-velocity measurements. Two alternative indicators for planetary searches. , 557:A93, September 2013. 29
- [48] C. P. Folsom, P. Petit, J. Bouvier, A. Lèbre, L. Amard, A. Palacios, J. Morin, J.-F. Donati, S. V. Jeffers, S. C. Marsden, and A. A. Vidotto. The evolution of surface magnetic fields in young solar-type stars - I. The first 250 Myr. , 457:580–607, March 2016. 12
- [49] P. Foukal, L. Bertello, W. C. Livingston, A. A. Pevtsov, J. Singh, A. G. Tlatov, and R. K. Ulrich. A Century of Solar Ca ii Measurements and Their Implication for Solar UV Driving of Climate. , 255:229–238, April 2009. 14

- [50] C. Fröhlich. Total solar irradiance variations since 1978. *Advances in Space Research*, 29:1409–1416, 2002. 13
- [51] Gaia Collaboration, T. Prusti, J. H. J. de Bruijne, A. G. A. Brown, A. Vallenari, C. Babusiaux, C. A. L. Bailer-Jones, U. Bastian, M. Biermann, D. W. Evans, and et al. The Gaia mission. , 595:A1, November 2016. 6
- [52] Michaël Gillon, Amaury H. M. J. Triaud, Brice-Olivier Demory, Emmanuël Jehin, Eric Agol, Katherine M. Deck, Susan M. Lederer, Julien de Wit, Artem Burdanov, James G. Ingalls, Emeline Bolmont, Jeremy Leconte, Sean N. Raymond, Franck Selsis, Martin Turbet, Khalid Barkaoui, Adam Burgasser, Matthew R. Burleigh, Sean J. Carey, Aleksander Chaushev, Chris M. Copperwheat, Laetitia Delrez, Catarina S. Fernandes, Daniel L. Holdsworth, Enrico J. Kotze, Valérie Van Grootel, Yaseen Almleaky, Zouhair Benkhaldoun, Pierre Magain, and Didier Queloz. Seven temperate terrestrial planets around the nearby ultracool dwarf star trappist-1. *Nature*, 542(7642):456–460, 02 2017. 5
- [53] P. A. Gilman. The tachocline and the solar dynamo. *Astronomische Nachrichten*, 326(3-4):208–217, 2005. 11
- [54] Gomes da Silva, J., Santos, N. C., Boisse, I., Dumusque, X., and Lovis, C. On the long-term correlation between the flux in the caii h k and h lines for fgk stars. *AA*, 566:A66, 2014. 31
- [55] Gomes da Silva, J., Santos, N. C., Bonfils, X., Delfosse, X., Forveille, T., and Udry, S. Long-term magnetic activity of a sample of m-dwarf stars from the harps program - i. comparison of activity indices. *AA*, 534:A30, 2011. 31
- [56] Gomes da Silva, J., Santos, N. C., Bonfils, X., Delfosse, X., Forveille, T., Udry, S., Dumusque, X., and Lovis, C. Long-term magnetic activity of a sample of m-dwarf stars from the harps program - ii. activity and radial velocity . *AA*, 541:A9, 2012. 31
- [57] David F. Gray and Artie P. Hatzes. Non-radial oscillation in the solar-temperature star 51 pegasi. *Astrophys. J.*, 490(1):412, 1997. 28
- [58] P. C. Gregory, S. M. Lawler, and B. Gladman. Additional Keplerian Signals in the HARPS data for Gliese 667C: Further Analysis. In M. Booth, B. C. Matthews, and J. R. Graham, editors, *Exploring the Formation and Evolution of Planetary Systems*, volume 299 of *IAU Symposium*, pages 287–288, January 2014. 7
- [59] Jeffrey C. Hall. Stellar chromospheric activity. *Living Reviews in Solar Physics*, 5(1):2, 2008. 30
- [60] K. L. Harvey and O. R. White. Magnetic and Radiative Variability of Solar Surface Structures. I. Image Decomposition and Magnetic-Intensity Mapping. , 515:812–831, April 1999. 29
- [61] A. P. Hatzes. The Radial Velocity Detection of Earth-mass Planets in the Presence of Activity Noise: The Case of α Centauri Bb. , 770:133, June 2013. 7

- [62] A. P. Hatzes. Periodic H α variations in GL 581: Further evidence for an activity origin to GL 581d. , 585:A144, January 2016. 30
- [63] Artie P. Hatzes. Simulations of stellar radial velocity and spectral line bisector variations: I. nonradial pulsations. *Publications of the Astronomical Society of the Pacific*, 108(728):839, 1996. 28, 29
- [64] Hatzes, A. P., Dvorak, R., Wuchterl, G., Guterman, P., Hartmann, M., Fridlund, M., Gandolfi, D., Guenther, E., and Pätzold, M. An investigation into the radial velocity variations of corot-7*. *AA*, 520:A93, 2010. 28
- [65] R. D. Haywood. *Hide and Seek: Radial-Velocity Searches for Planets around Active Stars*. PhD thesis, University of St Andrews, 2015. 20, 30
- [66] R. D. Haywood, A. Collier Cameron, Y. C. Unruh, C. Lovis, A. F. Lanza, J. Llama, M. Deleuil, R. Fares, M. Gillon, C. Moutou, F. Pepe, D. Pollacco, D. Queloz, and D. Segransan. The Sun as a planet-host star: proxies from SDO images for HARPS radial-velocity variations. *Monthly Notices of the Royal Astronomical Society*, 457(4):3637–3651, April 2016. 23
- [67] M. C. Johnson, M. Endl, W. D. Cochran, S. Meschiari, P. Robertson, P. J. MacQueen, E. J. Brugamyer, C. Caldwell, A. P. Hatzes, I. Ramírez, and R. A. Wittenmyer. A 12-year Activity Cycle for the Nearby Planet Host Star HD 219134. , 821:74, April 2016. 24
- [68] C. U. Keller, M. Schüssler, A. Vögler, and V. Zakharov. On the Origin of Solar Faculae. , 607:L59–L62, May 2004. 13
- [69] H. Kjeldsen, T. R. Bedding, R. P. Butler, J. Christensen-Dalsgaard, L. L. Kiss, C. McCarthy, G. W. Marcy, C. G. Tinney, and J. T. Wright. Solar-like Oscillations in α Centauri B. , 635:1281–1290, December 2005. 17
- [70] M. Konacki and A. Wolszczan. Masses and Orbital Inclinations of Planets in the PSR B1257+12 System. , 591:L147–L150, July 2003. 6
- [71] N. A. Krivova, S. K. Solanki, M. Fligge, and Y. C. Unruh. Reconstruction of solar irradiance variations in cycle 23: Is solar surface magnetism the cause? , 399:L1–L4, February 2003. 13
- [72] G. E. Kron. The Probable Detecting of Surface Spots on AR Lacertae B. , 59:261, October 1947. 31
- [73] A.-M. Lagrange, N. Meunier, M. Desort, and F. Malbet. Using the Sun to estimate Earth-like planets detection capabilities . III. Impact of spots and plages on astrometric detection. , 528:L9, April 2011. 22
- [74] Y. Lebreton and M. J. Goupil. Asteroseismology for “à la carte” stellar age-dating and weighing. Age and mass of the CoRoT exoplanet host HD 52265. , 569:A21, September 2014. 17
- [75] R. B. Leighton. Transport of Magnetic Fields on the Sun. , 140:1547, November 1964. 10

- [76] R. B. Leighton. A Magneto-Kinematic Model of the Solar Cycle. , 156:1, April 1969. 10
- [77] Jeffrey L. Linsky and Eugene H. Avrett. The solar h and k lines. *Publications of the Astronomical Society of the Pacific*, 82(485):169, 1970. 29
- [78] N. R. Lomb. Least-squares frequency analysis of unequally spaced data. , 39:447–462, February 1976. 32
- [79] C. Lovis and D. Fischer. *Radial Velocity Techniques for Exoplanets*, pages 27–53. December 2010. 24, 25, 27
- [80] C. Lovis, M. Mayor, F. Pepe, Y. Alibert, W. Benz, F. Bouchy, A. C. M. Correia, J. Laskar, C. Mordasini, D. Queloz, N. C. Santos, S. Udry, J.-L. Bertaux, and J.-P. Sivan. An extrasolar planetary system with three Neptune-mass planets. , 441:305–309, May 2006. 4
- [81] C. Lovis, D. Ségransan, M. Mayor, S. Udry, W. Benz, J.-L. Bertaux, F. Bouchy, A. C. M. Correia, J. Laskar, G. Lo Curto, C. Mordasini, F. Pepe, D. Queloz, and N. C. Santos. The HARPS search for southern extra-solar planets. XXVIII. Up to seven planets orbiting HD 10180: probing the architecture of low-mass planetary systems. , 528:A112, April 2011. 4, 30
- [82] V. V. Makarov, C. A. Beichman, J. H. Catanzarite, D. A. Fischer, J. Lebreton, F. Malbet, and M. Shao. Starspot Jitter in Photometry, Astrometry, and Radial Velocity Measurements. , 707:L73–L76, December 2009. 22
- [83] Sudip Mandal, Subhamoy Chatterjee, and Dipankar Banerjee. Association of plages with sunspots: A multi-wavelength study using kodaikanal ca ii k and greenwich sunspot area data. *The Astrophysical Journal*, 835(2):158, 2017. 14
- [84] P. J. D. Mauas. Building Reliable Models of M Dwarf Chromospheres: The Spectral Diagnostics. , 539:858–864, August 2000. 31
- [85] M. Mayor, C. Lovis, and N. C. Santos. Doppler spectroscopy as a path to the detection of Earth-like planets. , 513:328–335, September 2014. 7
- [86] M. Mayor and D. Queloz. A Jupiter-mass companion to a solar-type star. , 378:355–359, November 1995. 3, 4
- [87] Melo, C., Santos, N. C., Gieren, W., ki, G. Pietrzyn, Ruiz, M. T., a, S. G. Sou, Bouchy, F., Lovis, C., Mayor, M., Pepe, F., Queloz, D., da Silva, R., and Udry, S. A new neptune-mass planet orbiting hd219828. *AA*, 467(2):721–727, 2007. 29
- [88] Morais, M. H. M. and Correia, A. C. M. Stellar wobble caused by a binary system: Can it really be mistaken as an extra-solar planet? *AA*, 491(3):899–906, 2008. 25
- [89] A. Mortier and A. Collier Cameron. Stacked bayesian general lomb-scargle periodogram: identifying stellar activity signals. *Astronomy Astrophysics*, Forthcoming article, 2 2017. The research leading to these results received funding from the European Union Seventh Framework Programme (FP7/2007-2013) under grant agreement number 313014 (ETAEARTH). ACC acknowledges support from STFC grant ST/M001296/1. 33

- [90] Simon J. Murphy, Timothy R. Bedding, and Hiromoto Shibahashi. A planet in an 840 day orbit around a kepler main-sequence a star found from phase modulation of its pulsations. *The Astrophysical Journal Letters*, 827(1):L17, 2016. 6
- [91] Nardetto, N., Mourard, D., Kervella, P., Mathias, Ph., Mérand, A., and ier, D. Ber. High resolution spectroscopy for cepheids distance determination - i. line asymmetry. *AA*, 453(1):309–319, 2006. 29
- [92] England) NATO Advanced Research Workshop on the Theory of Sunspots (1991 : Cambridge, N. O. (Nigel Oscar) Weiss, 1941 Thomas, John H., and North Atlantic Treaty Organization. Scientific Affairs Division. Sunspots : theory and observations, 1992. "Proceedings of the NATO Advanced Research Workshop on the Theory of Sunspots, Cambridge, U.K., September 22-27, 1991"—T.p. verso. 25
- [93] M. B. Nielsen. *Differential Rotation in Sun-like Stars from Surface Variability and Asteroseismology*. 2017. 17
- [94] M. B. Nielsen, H. Schunker, L. Gizon, and W. H. Ball. Constraining differential rotation of Sun-like stars from asteroseismic and starspot rotation periods. , 582:A10, October 2015. 17
- [95] A. Nordlund, A. Brandenburg, R. L. Jennings, M. Rieutord, J. Ruokolainen, R. F. Stein, and I. Tuominen. Dynamo action in stratified convection with overshoot. , 392:647–652, June 1992. 19
- [96] R. W. Noyes, N. O. Weiss, and A. H. Vaughan. The relation between stellar rotation rate and activity cycle periods. , 287:769–773, December 1984. 24, 30
- [97] Mathieu Ossendrijver. The solar dynamo. *The Astronomy and Astrophysics Review*, 11(4):287–367, 2003. 11
- [98] S. J. O'Toole, C. G. Tinney, H. R. A. Jones, R. P. Butler, G. W. Marcy, B. Carter, and J. Bailey. Selection functions in doppler planet searches. , 392:641–654, January 2009. 32
- [99] Simon J. O'Toole, R. Paul Butler, C. G. Tinney, Hugh R. A. Jones, Geoffrey W. Marcy, Brad Carter, Chris McCarthy, Jeremy Bailey, Alan J. Penny, Kevin Apps, and Debra Fischer. New planets around three g dwarfs. *The Astrophysical Journal*, 660(2):1636, 2007. 32
- [100] C. E. Parnell, C. E. DeForest, H. J. Hagenaar, B. A. Johnston, D. A. Lamb, and B. T. Welsch. A Power-Law Distribution of Solar Magnetic Fields Over More Than Five Decades in Flux. , 698:75–82, June 2009. 19
- [101] F. Pepe, C. Lovis, D. Ségransan, W. Benz, F. Bouchy, X. Dumusque, M. Mayor, D. Queloz, N. C. Santos, and S. Udry. The HARPS search for Earth-like planets in the habitable zone. I. Very low-mass planets around $\text{\texttt{ASTROBJ}}\text{\texttt{HD 20794}}\text{\texttt{ASTROBJ}}$, $\text{\texttt{ASTROBJ}}\text{\texttt{HD 85512}}\text{\texttt{ASTROBJ}}$, and $\text{\texttt{ASTROBJ}}\text{\texttt{HD 192310}}\text{\texttt{ASTROBJ}}$. , 534:A58, October 2011. 4
- [102] M. Perryman. *The Exoplanet Handbook*. May 2011. 4, 28

- [103] Michael Perryman, Joel Hartman, GÃ¡jspÃ¡r Á. Bakos, and Lennart Lindegren. Astrometric exoplanet detection with gaia. *The Astrophysical Journal*, 797(1):14, 2014. 6
- [104] A. A. Pevtsov, I. Virtanen, K. Mursula, A. Tlatov, and L. Bertello. Reconstructing solar magnetic fields from historical observations. I. Renormalized Ca K spectro-heliograms and pseudo-magnetograms. , 585:A40, January 2016. 29
- [105] N. Pizzolato, A. Maggio, G. Micela, S. Sciortino, and P. Ventura. The stellar activity-rotation relationship revisited: Dependence of saturated and non-saturated X-ray emission regimes on stellar mass for late-type dwarfs. , 397:147–157, January 2003. 31
- [106] P. Plavchan, D. Latham, S. Gaudi, J. Crepp, X. Dumusque, G. Furesz, A. Vanderburg, C. Blake, D. Fischer, L. Prato, R. White, V. Makarov, G. Marcy, K. Stapelfeldt, R. Haywood, A. Collier-Cameron, A. Quirrenbach, S. Mahadevan, G. Anglada, and P. Muirhead. Radial Velocity Prospects Current and Future: A White Paper Report prepared by the Study Analysis Group 8 for the Exoplanet Program Analysis Group (ExoPAG). *ArXiv e-prints*, March 2015. 22, 23
- [107] D. Queloz. Echelle Spectroscopy with a CCD at Low Signal-To-Noise Ratio. In A. G. D. Philip, K. Janes, and A. R. Upgren, editors, *New Developments in Array Technology and Applications*, volume 167 of *IAU Symposium*, page 221, 1995. 27
- [108] Queloz, D., Bouchy, F., Moutou, C., Hatzes, A., Hébrard, G., Alonso, R., Auvergne, M., Baglin, A., Barbieri, M., Barge, P., Benz, W., Bordé, P., Deeg, H. J., Deleuil, M., Dvorak, R., Erikson, A., Ferraz Mello, S., Fridlund, M., Gandolfi, D., Gillon, M., Guenther, E., Guillot, T., Jorda, L., Hartmann, M., Lammer, H., Léger, A., Llebaria, A., Lovis, C., Magain, P., Mayor, M., Mazeh, T., Ollivier, M., Pätzold, M., Pepe, F., Rauer, H., Rouan, D., Schneider, J., Segransan, D., Udry, S., and Wuchterl, G. The corot-7planetary system: two orbiting super-earths. *AA*, 506(1):303–319, 2009. 28, 30
- [109] Queloz, D., Henry, G. W., Sivan, J. P., Baliunas, S. L., Beuzit, J. L., Donahue, R. A., Mayor, M., Naef, D., Perrier, C., and Udry, S. No planet for hd 166435. *AA*, 379(1):279–287, 2001. 28
- [110] V. Rajpaul, S. Aigrain, and S. Roberts. Ghost in the time series: no planet for Alpha Cen B. , 456:L6–L10, February 2016. 7
- [111] H. Rauer, C. Catala, C. Aerts, T. Appourchaux, W. Benz, A. Brandeker, J. Christensen-Dalsgaard, M. Deleuil, L. Gizon, M.-J. Goupil, M. Güdel, E. Janot-Pacheco, M. Mas-Hesse, I. Pagano, G. Piotto, D. Pollacco, C. Santos, A. Smith, J.-C. Suárez, R. Szabó, S. Udry, V. Adibekyan, Y. Alibert, J.-M. Almenara, P. Amaro-Seoane, M. A.-v. Eiff, M. Asplund, E. Antonello, S. Barnes, F. Baudin, K. Belkacem, M. Bergemann, G. Bihain, A. C. Birch, X. Bonfils, I. Boisse, A. S. Bonomo, F. Borsa, I. M. Brandão, E. Brocato, S. Brun, M. Burleigh, R. Burston, J. Cabrera, S. Cassisi, W. Chaplin, S. Charpinet, C. Chiappini, R. P. Church, S. Csizmadia, M. Cunha, M. Damasso, M. B. Davies, H. J. Deeg, R. F. Díaz, S. Dreizler, C. Dreyer, P. Eggenberger, D. Ehrenreich, P. Eigmüller, A. Erikson,

- R. Farmer, S. Feltzing, F. de Oliveira Fialho, P. Figueira, T. Forveille, M. Fridlund, R. A. García, P. Giommi, G. Giuffrida, M. Godolt, J. Gomes da Silva, T. Granzer, J. L. Grenfell, A. Grotsch-Noels, E. Günther, C. A. Haswell, A. P. Hatzes, G. Hébrard, S. Hekker, R. Helled, K. Heng, J. M. Jenkins, A. Johansen, M. L. Khodachenko, K. G. Kislyakova, W. Kley, U. Kolb, N. Krivova, F. Kupka, H. Lammer, A. F. Lanza, Y. Lebreton, D. Magrin, P. Marcos-Arenal, P. M. Marrese, J. P. Marques, J. Martins, S. Mathis, S. Mathur, S. Messina, A. Miglio, J. Montalban, M. Montalto, M. J. P. F. G. Monteiro, H. Moradi, E. Moravveji, C. Mordasini, T. Morel, A. Mortier, V. Nascimbeni, R. P. Nelson, M. B. Nielsen, L. Noack, A. J. Norton, A. Ofir, M. Oshagh, R.-M. Ouazzani, P. Pápics, V. C. Parro, P. Petit, B. Plez, E. Poretti, A. Quirrenbach, R. Ragazzoni, G. Raimondo, M. Rainer, D. R. Reese, R. Redmer, S. Reffert, B. Rojas-Ayala, I. W. Roxburgh, S. Salmon, A. Santerne, J. Schneider, J. Schou, S. Schuh, H. Schunker, A. Silva-Valio, R. Silvotti, I. Skillen, I. Snellen, F. Sohl, S. G. Sousa, A. Sozzetti, D. Stello, K. G. Strassmeier, M. Švanda, G. M. Szabó, A. Tkachenko, D. Valencia, V. Van Grootel, S. D. Vauclair, P. Ventura, F. W. Wagner, N. A. Walton, J. Weingrill, S. C. Werner, P. J. Wheatley, and K. Zwintz. The PLATO 2.0 mission. *Experimental Astronomy*, 38:249–330, November 2014. 8
- [112] A. Reiners. Activity-induced radial velocity jitter in a flaring M dwarf. , 498:853–861, May 2009. 22
- [113] Ansgar Reiners. Observations of cool-star magnetic fields. *Living Reviews in Solar Physics*, 9(1):1, 2012. 11, 31
- [114] G. R. Ricker, J. N. Winn, R. Vanderspek, D. W. Latham, G. Á. Bakos, J. L. Bean, Z. K. Berta-Thompson, T. M. Brown, L. Buchhave, N. R. Butler, R. P. Butler, W. J. Chaplin, D. Charbonneau, J. Christensen-Dalsgaard, M. Clampin, D. Deming, J. Doty, N. De Lee, C. Dressing, E. W. Dunham, M. Endl, F. Fressin, J. Ge, T. Henning, M. J. Holman, A. W. Howard, S. Ida, J. Jenkins, G. Jernigan, J. A. Johnson, L. Kaltenegger, N. Kawai, H. Kjeldsen, G. Laughlin, A. M. Levine, D. Lin, J. J. Lissauer, P. MacQueen, G. Marcy, P. R. McCullough, T. D. Morton, N. Narita, M. Paegert, E. Palle, F. Pepe, J. Pepper, A. Quirrenbach, S. A. Rinehart, D. Sasselov, B. Sato, S. Seager, A. Sozzetti, K. G. Stassun, P. Sullivan, A. Szentgyorgyi, G. Torres, S. Udry, and J. Villaseñor. Transiting Exoplanet Survey Satellite (TESS). In *Space Telescopes and Instrumentation 2014: Optical, Infrared, and Millimeter Wave*, volume 9143 of , page 914320, August 2014. 7
- [115] Paul Robertson, Michael Endl, William D. Cochran, and Sarah E. Dodson-Robinson. H activity of old m dwarfs: Stellar cycles and mean activity levels for 93 low-mass stars in the solar neighborhood. *The Astrophysical Journal*, 764(1):3, 2013. 30
- [116] Paul Robertson, Michael Endl, William D. Cochran, and Sarah E. Dodson-Robinson. H activity of old m dwarfs: Stellar cycles and mean activity levels for 93 low-mass stars in the solar neighborhood. *The Astrophysical Journal*, 764(1):3, 2013. 31

- [117] Paul Robertson, Michael Endl, Gregory W. Henry, William D. Cochran, Phillip J. MacQueen, and Michael H. Williamson. Stellar activity and its implications for exoplanet detection on gj176. *The Astrophysical Journal*, 801(2):79, 2015. 31
- [118] Paul Robertson, Suvrath Mahadevan, Michael Endl, and Arpita Roy. Stellar activity masquerading as planets in the habitable zone of the m dwarf gliese 581. *Science*, 345(6195):440–444, 2014. 30, 31
- [119] Paul Robertson, Arpita Roy, and Suvrath Mahadevan. Stellar activity mimics a habitable-zone planet around kapteyn’s star. *The Astrophysical Journal Letters*, 805(2):L22, 2015. 20, 31
- [120] R. M. Roettenbacher, J. D. Monnier, H. Korhonen, A. N. Aarnio, F. Baron, X. Che, R. O. Harmon, Zs. Kővári, S. Kraus, G. H. Schaefer, G. Torres, M. Zhao, T. A. ten Brummelaar, J. Sturmann, and L. Sturmann. No sun-like dynamo on the active star andromedae from starspot asymmetry. *Nature*, 533(7602):217–220, 05 2016. 12
- [121] S. H. Saar. The Radial Velocity Effects of Stellar Surface Phenomena. In E. Stempeis, editor, *15th Cambridge Workshop on Cool Stars, Stellar Systems, and the Sun*, volume 1094 of *American Institute of Physics Conference Series*, pages 152–161, February 2009. 22
- [122] Santos, N. C., Mayor, M., Naef, D., Pepe, F., Queloz, D., Udry, S., Burnet, M., en, J. V. Clau, Helt, B. E., en, E. H. Ol, and Pritchard, J. D. The coralie survey for southern extra-solar planets - ix. a 1.3-day period brown dwarf disguised as a planet. *AA*, 392(1):215–229, 2002. 25
- [123] J. D. Scargle. Studies in astronomical time series analysis. II - Statistical aspects of spectral analysis of unevenly spaced data. , 263:835–853, December 1982. 32
- [124] C. J. Schrijver and K. L. Harvey. The distribution of solar magnetic fluxes and the nonlinearity of stellar flux-flux relations. , 343:481–488, August 1989. 14
- [125] H. C. Spruit. Pressure equilibrium and energy balance of small photospheric flux-tubes. , 50:269–295, December 1976. 13
- [126] H. C. Spruit. Heat flow near obstacles in the solar convection zone. , 55:3–34, November 1977. 13
- [127] R. F. Stein and A. Nordlund. Topology of convection beneath the solar surface. , 342:L95–L98, July 1989. 18
- [128] Robert F. Stein. Solar surface magneto-convection. *Living Reviews in Solar Physics*, 9(1):4, 2012. 18, 19
- [129] Dennis Stello, William J. Chaplin, Hans Bruntt, Orlagh L. Creevey, Antonio García-Hernández, Mario J. P. F. G. Monteiro, Andrés Moya, Pierre-Olivier Quirion, Sergio G. Sousa, Juan-Carlos Suárez, Thierry Appourchaux, Torben Arentoft, Jerome Ballot, Timothy R. Bedding, Jørgen Christensen-Dalsgaard,

- Yvonne Elsworth, Stephen T. Fletcher, Rafael A. García, Günter Houdek, Sebastian J. Jiménez-Reyes, Hans Kjeldsen, Roger New, Clara Régulo, David Salabert, and Thierry Toutain. Radius determination of solar-type stars using asteroseismology: What to expect from the kepler mission. *The Astrophysical Journal*, 700(2):1589, 2009. 17
- [130] A. Suárez Mascareño, R. Rebolo, J. I. González Hernández, and M. Esposito. Characterisation of the radial velocity signal induced by rotation in late-type dwarfs. *ArXiv e-prints*, March 2017. 30
- [131] A. Suárez Mascareño, R. Rebolo, J. I. González Hernández, and M. Esposito. Rotation periods of late-type dwarf stars from time series high-resolution spectroscopy of chromospheric indicators. *Monthly Notices of the Royal Astronomical Society*, 452(3):2745, 2015. 30
- [132] L. M. Thornton and C. E. Parnell. Small-scale flux emergence observed using hinode/sot. *Solar Physics*, 269(1):13–40, 2011. 19
- [133] C. G. Toner and D. F. Gray. The starpatch on the G8 dwarf XI Bootis A. , 334:1008–1020, November 1988. 28
- [134] A. H. Vaughan, G. W. Preston, and O. C. Wilson. Flux measurements of ca ii and k emission. *Publications of the Astronomical Society of the Pacific*, 90(535):267, 1978. 30
- [135] A. Vögler and M. Schüssler. A solar surface dynamo. , 465:L43–L46, April 2007. 19
- [136] S. R. Walton, D. G. Preminger, and G. A. Chapman. The Contribution of Faculae and Network to Long-Term Changes in the Total Solar Irradiance. , 590:1088–1094, June 2003. 13
- [137] O. C. Wilson. A Probable Correlation Between Chromospheric Activity and Age in Main-Sequence Stars. , 138:832, October 1963. 24
- [138] P. R. Wilson. Sunspots. r. j. bray and r. e. loughhead. wiley, new york, 1965. xvi + 303 pp. illus. 13.75. *Science*, 149(3679) : 46 – – 46, 1965. 25
- [139] A. Wolszczan and D. A. Frail. A planetary system around the millisecond pulsar PSR1257 + 12. , 355:145–147, January 1992. 3, 6
- [140] D. J. Wright, R. A. Wittenmyer, C. G. Tinney, J. S. Bentley, and J. Zhao. Three Planets Orbiting Wolf 1061. , 817:L20, February 2016. 4
- [141] Zechmeister, M. and Kürster, M. The generalised lomb-scargle periodogram - a new formalism for the floating-mean and keplerian periodograms. *AA*, 496(2):577–584, 2009. 32
- [142] Zucker, S., Mazeh, T., Santos, N. C., Udry, S., and Mayor, M. Multi-order todcor: Application to observations taken with the coralie echelle spectrograph - ii. a planet in the system hdâ41004. *AA*, 426(2):695–698, 2004. 25